A Pilot Experimental Study on the Low Cycle Fatigue Behavior of Stainless Steel Rebars for Earthquake Engineering Applications

by
Yihui Zhou, Yu-Chen Ou, George C. Lee, and Jerome S. O'Connor
University at Buffalo

August, 2008

ABSTRACT

The use of stainless steel reinforcing bars in reinforced concrete structures is one of the promising solutions to corrosion issues. For stainless steel reinforcing bars to be used in seismic applications, several mechanical properties need to be investigated such as nominal and actual yield strengths, tensile strengths, elongations and low cycle fatigue behavior. A research task was initiated at MCEER to experimentally investigate the above mentioned mechanical properties of various types of stainless steel reinforcing bars that are currently available in the market. Steels tested include 316LN, Enduramet 32, and 2205 Duplex. They were compared against A706 G60 carbon steel reinforcing bars, which are typical for seismic applications, and MMFX II, which is a high strength, corrosion resistant steel that has recently appeared on the market. Low-cycle fatigue tests of the bars were conducted under strain control with constant amplitude to obtain the strain life models of the bars. Electron microscope photos were taken to the specimen failure sections of different types of the steels to observe the fatigue characteristics. The tests results show that the stainless steel rebar is much more ductile than A706 G60 and MMFX II, and MMFX II is least capable of elongating among the steels tested. Mean strain has little effect on the fatigue life and hence mean strain effects could be ignored in the engineering application. The equation proposed by Mander is too conservative in estimating the fatigue life for Enduramet 32, 316LN, and 2205 duplex stainless steels, A706 G60 rebar and MMFX II rebar. Enduramet 32 has the highest ductility and the best low-cycle fatigue performance among the steels investigated. In general, the three types of stainless steel are better than A706 G60.

ACKNOWLEDGEMENTS

Financial support for this project provided by private industry through MCEER, University at Buffalo. The support of International Molybdenum Association, Nickel Institute, Talley Metals - A Carpenter Company, North American Stainless and Salit Specialty Steel is sincerely appreciated. Dr. Frank Smith, P. Eng. served as project manager for the consortium. Many thanks also go to the technical staff in the SEESL for their consistent assistance during the experiment: Mr. Mark Pitman, Mr. Duane Kozlowski, Mr. Scott Weinreber, Mr. Robert Staniszewski, Mr. Christopher Budden and Mr. Gary Majewski.

TABLE OF CONTENTS

CHAPTER **PAGE**

LIST OF FIGURES

FIGURE **PAGE**

LISTS OF TABLES

TABLE **PAGE**

CHAPTER 1
INTRODUCTION

1.1 Objectives

Corrosion of structural steel and concrete reinforcing steel has contributed to the premature failure of highway bridge decks, columns and superstructures and shortened their service lives. Two important causes for corrosion of rebar are chloride attack due to deicing salts and seawater and carbonation of concrete due to carbonic acid from carbon dioxide. While chloride-induced corrosion is generally more pernicious and expensive to repair, carbonation-induced corrosion of reinforcement may affect a far wider range of reinforced concrete structures. Solid stainless steel rebar is a promising solution to address these issues because of its superior corrosion resistance compared to carbon steel and surface treated corrosion resistant steel such as epoxy coated rebar, galvanized rebar, and stainless clad rebar (Smith, 2007).

Despite its higher cost, the use of solid stainless steel rebar in bridges and highways has been growing over the past 20 years. However, its use in seismic applications is still limited because its seismic performance is not well understood. Current seismic design practice of reinforced concrete structures allows reinforcing steel to undergo large inelastic tension strain reversals when resisting earthquake-induced forces. Low cycle fatigue is defined as a fatigue life of less than 10^5 cycles (Stephens et al., 2001) and little knowledge exists regarding the low-cycle fatigue behavior of stainless steel rebar. This report presents the results of the low-cycle fatigue tests of three types of stainless steel rebar in addition to A706 G60 carbon steel rebar and MMFX II rebar. Other mechanical properties associated with seismic design are also presented including yield strengths, elongations, actual and specified yield strengths, and ratios of tensile to yield strengths.

1.2 Stainless Steel

Stainless steel is metallurgic ally defined as a ferrous alloy with a minimum of 11% chromium content according to ASTM A955 (ASTM, 2004). Such steels have higher resistance to oxidation (rust) and corrosion in several environments. Stainless steel is commonly divided into five groups: martenistic stainless steels, ferritic stainless steels, austenitic stainless steels, duplex (ferritic-austenitic) stainless steels, and precipitation-hardening stainless steels (Heiyantuduwa et al., 2006; Sakumoto et al., 1996).

1.3 Fatigue Strain-Life Relationship

Previous studies by Tong et al. (1989) and Lefebvre and Ellyin (1984) have indicated that for a fully reversed constant-strain-controlled test, there is negligible variation in the cyclic hysteresis energy with the number of cycles during fatigue life. As shown in Figure 1-1, the hysteresis energy of the cycle at half-life can be used as a characteristic of the entire test (Mander et al., 1994).

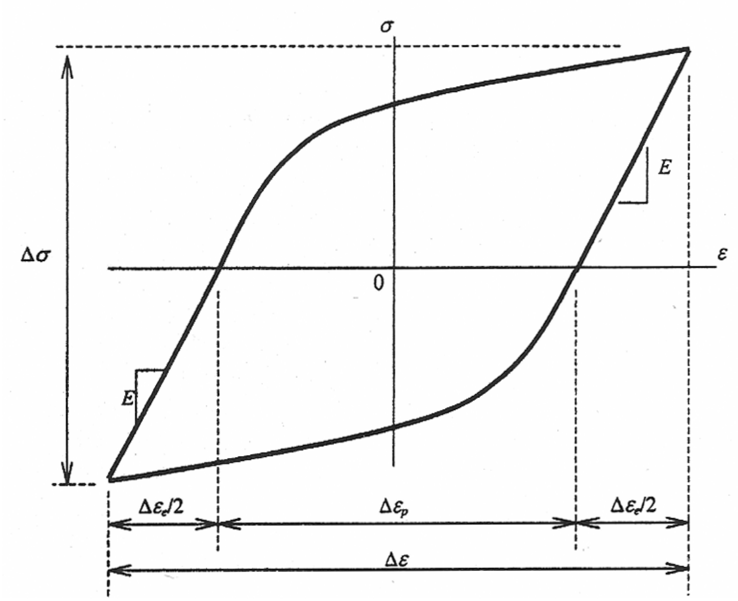

Figure 1-1: Stable Cyclic Stress-Strain Hysteresis Loop (Stephens et al., 2001)

The total strain amplitude can be resolved into elastic and plastic components, each of which has been shown to be correlated with fatigue life in a linear model using a log-log scale for most metals as presented in Figure 1-2. The Coffin-Manson law (Manson, 1953; Coffin, 1954) relates the plastic strain amplitude to the number of reversals to failure and when combined with an elastic term, and the relationship is illustrated in Equation 1-1.

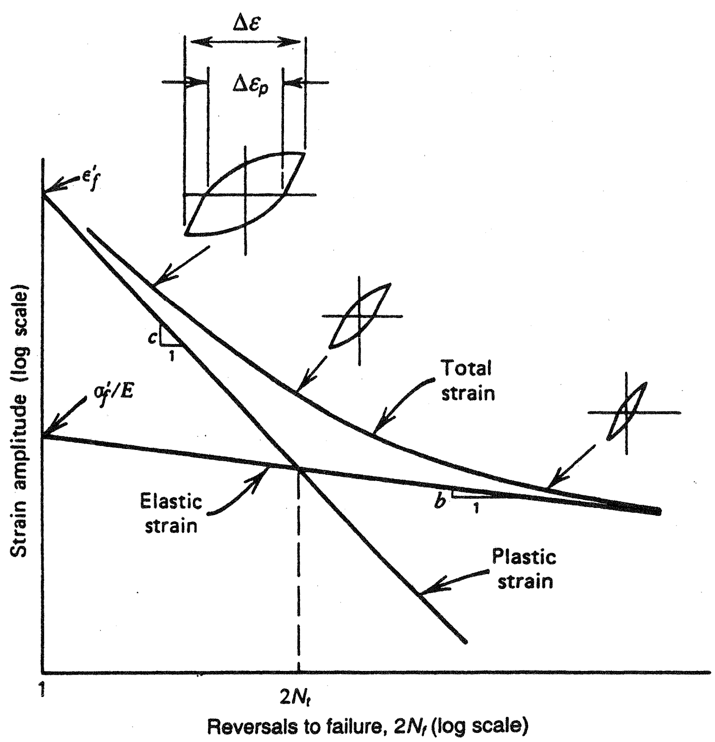

Figure 1-2: Strain-Life Curves Showing Total, Elastic, and Plastic Strain Components (Stephens et al., 2001)

$$\frac{\Delta\varepsilon}{2} = \frac{\sigma_f\,'}{E}(2N_f)^b + \varepsilon_f\,'(2N_f)^c \qquad (1\text{-}1)$$

where

$(\Delta\varepsilon / 2)$ = total strain amplitude

$2N_f$ = reversals to failure (1 reversal = 0.5 cycles)

$\sigma_f\,'$ = fatigue strength coefficient

b = fatigue strength exponent

$\varepsilon_f\,'$ = fatigue ductility coefficient

c = fatigue ductility exponent

E = modulus of elasticity

CHAPTER 2
TEST SET UP AND LOAD HISTORY

2.1 Equipment and Instrumentation

The steel coupon tests for monotonic tension and cyclic low cycle fatigue were conducted on the MTS fabricated load frame assembly 309.40 as photographed in Figure 2-1. This MTS servo-controlled closed-loop load frame at University at Buffalo has a load capacity of 110 kips/500 kN. Two types of MTS extensometers were attached to the gage length of the specimens to control and measure strains in the gage length for the monotonic tension test and the low cycle fatigue test, respectively. As shown in figures 2-2 and 2-3, respectively, the extensometer of MTS model No. 632.25E-20, which has a capacity of $\pm 1in$, was used for the monotonic tension tests, and the extensometer of MTS model No.632.11B-20, which is capable of measuring up to $\pm 0.15in$, was utilized in the low cycle fatigue tests.

Figure 2-1: Load Frame

(a)

(b)

Figure 2-2: (a) A Specimen before Monotonic Tension Test; (b) A Failed Monotonic Tension Test Specimen

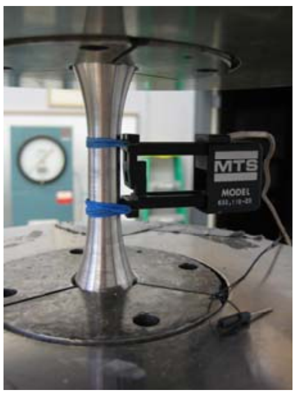

(a)

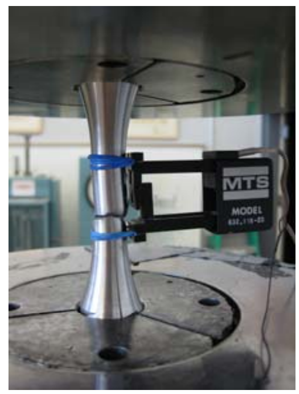

(b)

Figure 2-3: (a) A Specimen before Fatigue Test; (b) A Failed Fatigue Test Specimen

2.2 Specimen Design

Monotonic tension tests were carried out to determine some basic mechanical factors for the different types of steel being investigated. These included Young's modulus (E), yield strain (ε_y), yield strength (σ_y), ultimate strain (ε_u) and tensile strength (σ_u). The specimen for the monotonic tests was designed according to ASTM E8 (ASTM, 2004) and is shown in Figure 2-4.

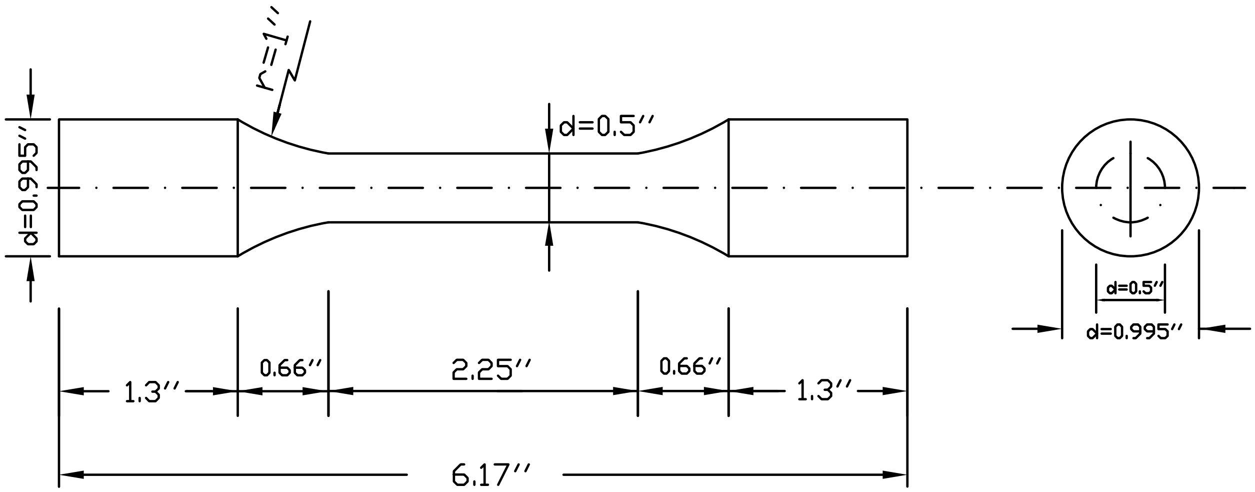

Figure 2-4: Monotonic Tension Test Specimen

The specimen for low-cycle fatigue was designed according to ASTM E606 (ASTM, 2004) and is shown in Figure 2-5.

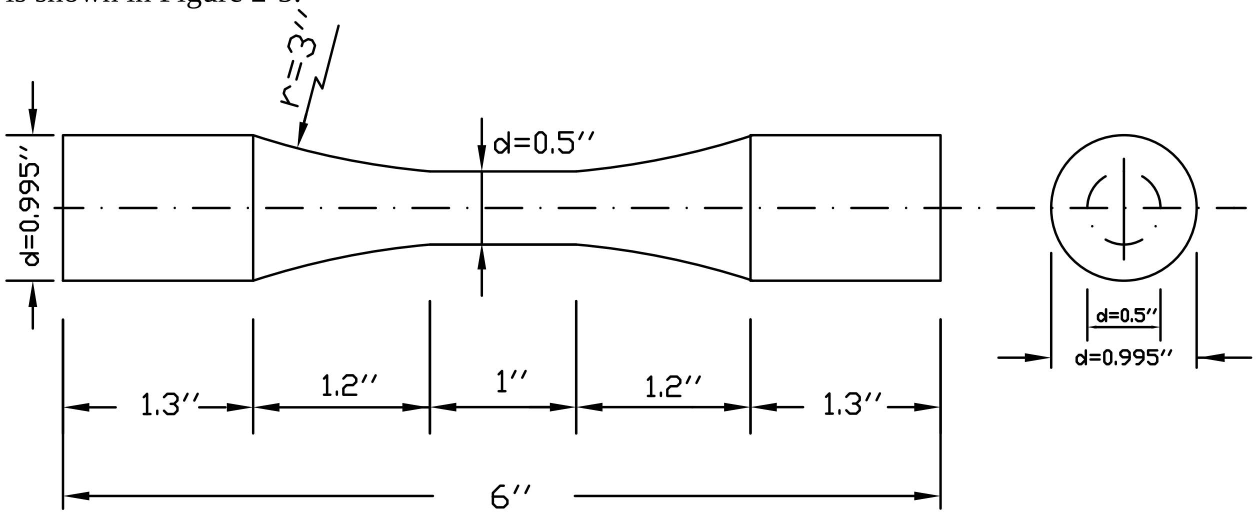

Figure 2-5: Fatigue Test Specimen

2.3 Steel Material Details

Enduramet 32 rebar, 316LN rebar, and 2205 Duplex, designated as S24100, S31653 and S31803 in ASTM A955 (ASTM, 2004), respectively, were the three types of stainless steel rebar tested in this experiment. Carbon steel rebar (A706 G60) which is typical for seismic design, and MMFX II, a high strength steel which has recently been introduced on the market were tested for comparison. The chemical compositions, mechanical properties and photos of the steel are presented in Tables 2-1 and 2-2 and Figure 2-6, respectively.

Table 2-1: Chemical Compositions of Steels Investigated

Steel Name	Chemical Composition (wt%)												
	C	Mn	Si	P	S	Cr	Ni	Mo	Cu	Co	N	B	C Eqv
Enduramet 32	0.05	12.0	0.36	0.019	0.002	17.4	0.75	0.14	0.07	0.03	0.30	0.0021	3.826
316 LN	0.014	1.37	0.80	0.024	0.001	17.87	10.17	2.06	0.25	0.13	0.15	0.0028	2.503
2205 Duplex	0.02	1.72	0.46	0.024	0.002	21.39	4.74	2.69	0.33	-----	0.17	0.0022	2.637
A706 G60	0.29	1.22	0.23	0.005	0.040	0.13	0.10	0.030	0.39	-----	-----	-----	0.517
MMFX II	0.07	0.45	0.14	0.01	0.012	9.98	0.09	0.009	0.08	-----	-----	-----	1.148
The equivalent carbon content is calculated according to ASTM A706 (ASTM, 2004).													

Table 2-2: Mechanical Properties of Steels Investigated

Steel Name	UNS	Producer	Size in. (mm)	Specified Yield Stress (ksi)
Enduramet 32	S24100	Talley Metals	1.001000 (25.42)	75
2205 Duplex	S31803	Talley Metals	1.001000 (25.42)	75
316 LN	S31653	Talley Metals	1.001000 (25.42)	75
A706 G60	------	Gerdau Ameristeel	(25)	60
MMFX II	------	MMFX Technology Corp.	1.001000 (25.42)	100

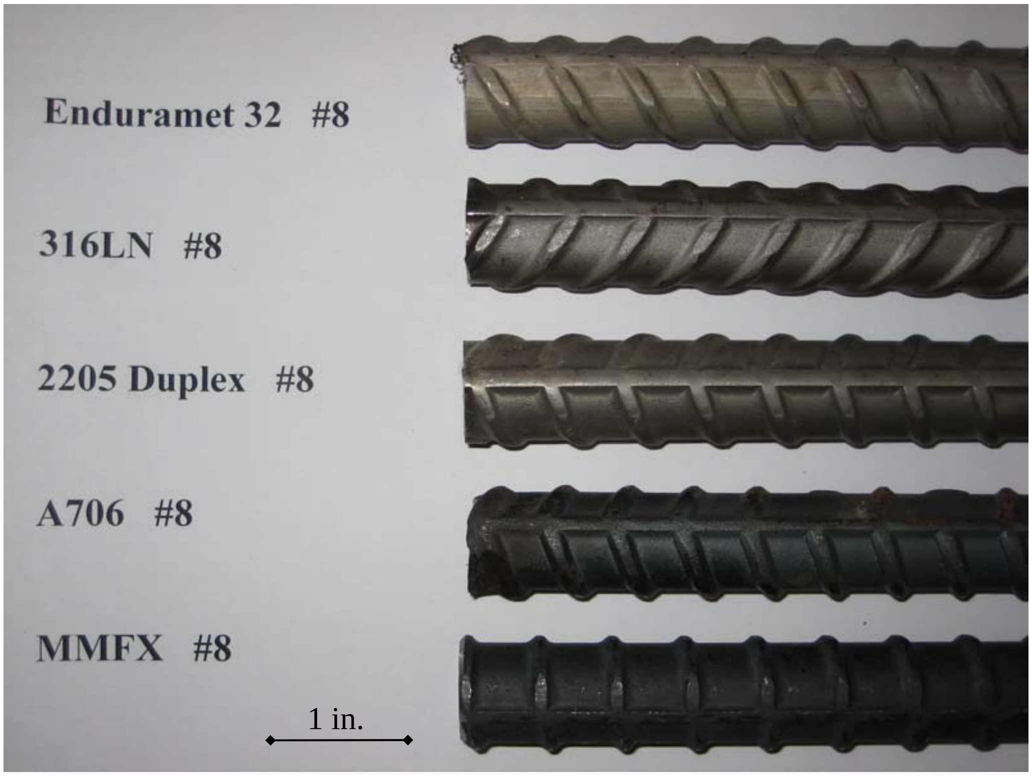

Figure 2-6: Raw Rebar Specimens

2.4 Loading History

Previous researchers reached a conclusion that the fatigue life for a given strain amplitude measured under cyclic loading with a constant amplitude, without high preloads, is independent of the level of the mean stress or mean strain (Pellissier-Tanon et al., 1982). The strain ratio, R, is defined as Equation 2-1

$$R = \varepsilon_{\min} / \varepsilon_{\max} \tag{2-1}$$

where $\varepsilon_{\min}$ and $\varepsilon_{\max}$ are the largest compressive and tensile strains respectively, with a sign convention of tension-positive. The mean strain, ε_m, is defined as Equation 2-2

$$\varepsilon_m = \frac{\varepsilon_{\max} + \varepsilon_{\min}}{2} \tag{2-2}$$

$R = -1$ is the focus of this test. However, tests with values of R in other positive and negative regions were also carried out in order to verify the theory mentioned above. The strain rate used was 0.005/sec (Mander et al., 1994). The loading protocol is shown in Figure 2-7.

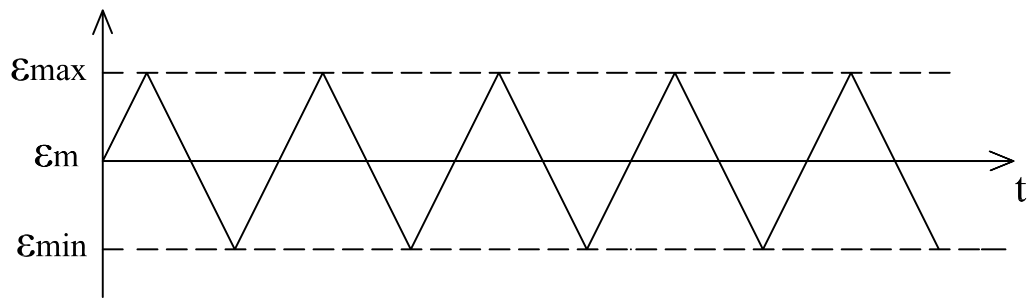

Figure 2-7: Constant Amplitude Straining Schematic

In reinforced concrete structures, both concrete and transverse reinforcement can help prevent buckling of the longitudinal rebar in compression. Thus, buckling of the rebar was prevented during tests. This was achieved by setting a limit on the strain level. Empirical stress-strain data from carbon steel was used to estimate the maximum strain the specimen could experience without significant buckling. Through trial calculations, 0.025 (2.5%) was found to be the upper limit below which buckling of the specimens would not occur.

CHAPTER 3
EXPERIMENTAL RESULTS

3.1 Monotonic Tension Test Results

Figure 3-1 presents stress-strain curves from the monotonic tests. The major characteristic stress-strain control factors for each single material type are listed in Table 3-1. In the table, the actual yield strengths determined by the 0.2% offset method per ASTM E8 and the 0.35 percent strain method per ACI 318 (ACI, 2005) were denoted as σ_{y1} and σ_{y2}, respectively.

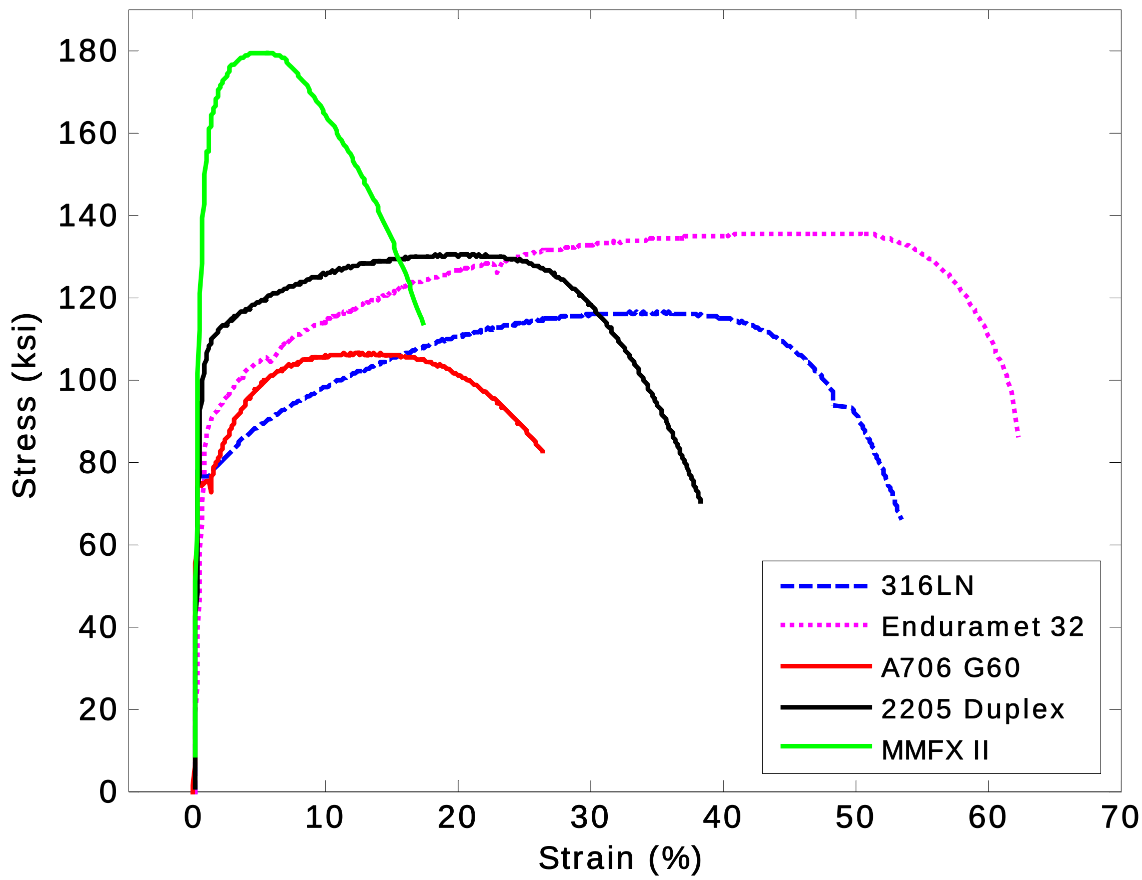

Figure 3-1: Stress-Strain Results for Monotonic Tension Test

Table 3-1: Monotonic Tension Test Results

	E (ksi)	Specified σ_y (ksi)	Actual σ_{y1} (ksi)	Actual σ_{y2} (ksi)	Actual σ_u (ksi)	$\frac{\sigma_u}{\sigma_{y2}}$	Elongation (%)
Enduramet 32	29848	75	84.17	83.52	136.25	1.63	58.66
316LN	28981	75	77.14	77.75	116.34	1.50	52.82
2205 Duplex	27705	75	94.06	96.97	130.53	1.35	38.74
A706 G60	30244	60	73.67	72.59	106.02	1.46	26.5
MMFX II	31533	100	137.88	100.73	179.43	1.78	17.51

σ_{y1} is determined by 0.2% offset method according to ASTM E 8 (ASTM, 2004).

σ_{y2} is defined as the stress corresponding to a strain of 0.35 percent (ACI 318-05, 2005).

Test results show that, compared to carbon steel, the Young's modulus (E) of the three types of stainless steel rebar are slightly smaller, and slightly higher for MMFX II. The values of E of Enduramet 32 rebar, 316 LN rebar, 2205 duplex rebar and MMFX II rebar are 98.7%, 95.8%, 91.6% and 104.3% that of A706 G60 rebar, respectively. According to the latest ACI 318 code, reinforcement in members resisting earthquake-induced forces should have values of σ_u / σ_{y2} no less than 1.25. Furthermore, the actual yield strength should exceed the specified yield strength no more than 18 ksi. Enduramet 32 rebar, 316LN rebar, 2205 duplex rebar and MMFX II rebar all meet these requirements. Among the five types of steel tested, MMFX II has the highest yielding stress $\sigma_{y2} = 100.73 ksi$. Although the use of rebar of higher yield strength may reduce structural member sizes, it tends to increase crack widths and deflections under service loads, causing problems of serviceability. Under monotonic loading, the elongations at fracture of the three types of stainless steel rebar are substantially higher than A706 G60 rebar and MMFX II rebar. Except for the stainless steels, the elongation of A706 G60 (26.5%) is also higher than that of MMFX II (17.51%). This shows that the stainless steel rebar is much more ductile than A706 G60 and MMFX II, and MMFX II is least capable of elongating among the steels tested.

3.2 Cyclic Stress-Strain Behavior

Three complete fatigue test results and their representative loops (total strain vs. stress) for Enduramet 32 rebar, including the cases of zero mean strain ($R = -1$), positive mean strain ($R > -1$) and negative mean strain ($R < -1$), are presented in Figures 3-2, 3-3 and 3-4, respectively.

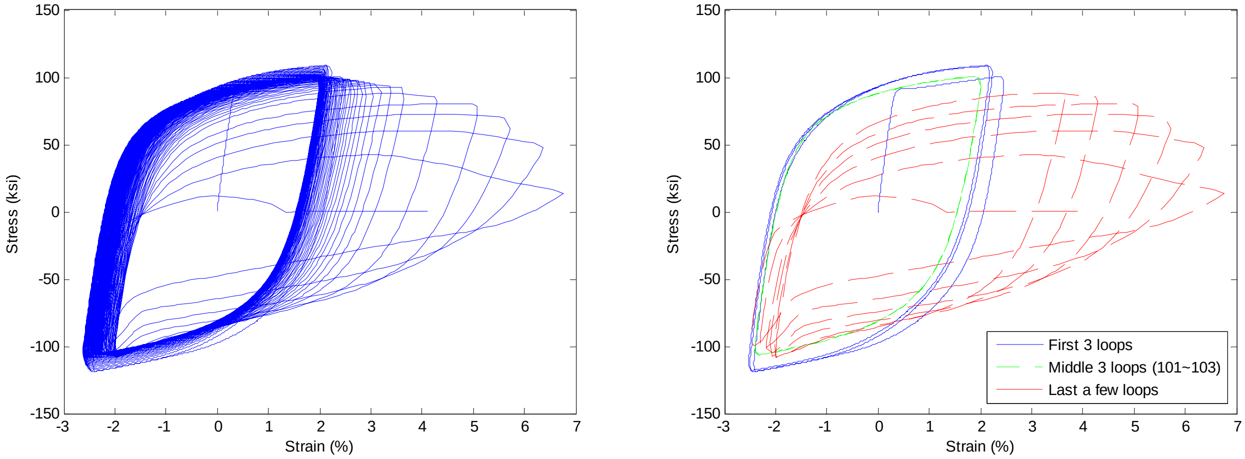

(a) (b)

Figure 3-2: Low-Cycle Fatigue Hysteresis Loops for Enduramet 32 at Strain Amplitude 2.238% (R=-1)
(a). Whole Loops (b). Loop Extract

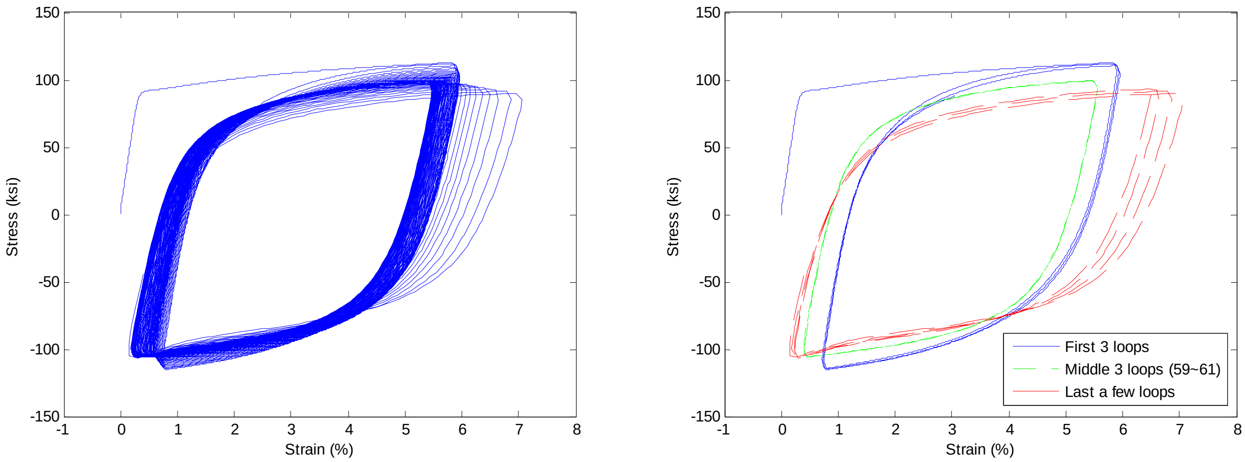

(a) (b)

Figure 3-3: Low-Cycle Fatigue Hysteresis Loops for Enduramet 32 at Strain Amplitude 2.608% (R>-1)
(a). Whole Loops (b). Loop Extract

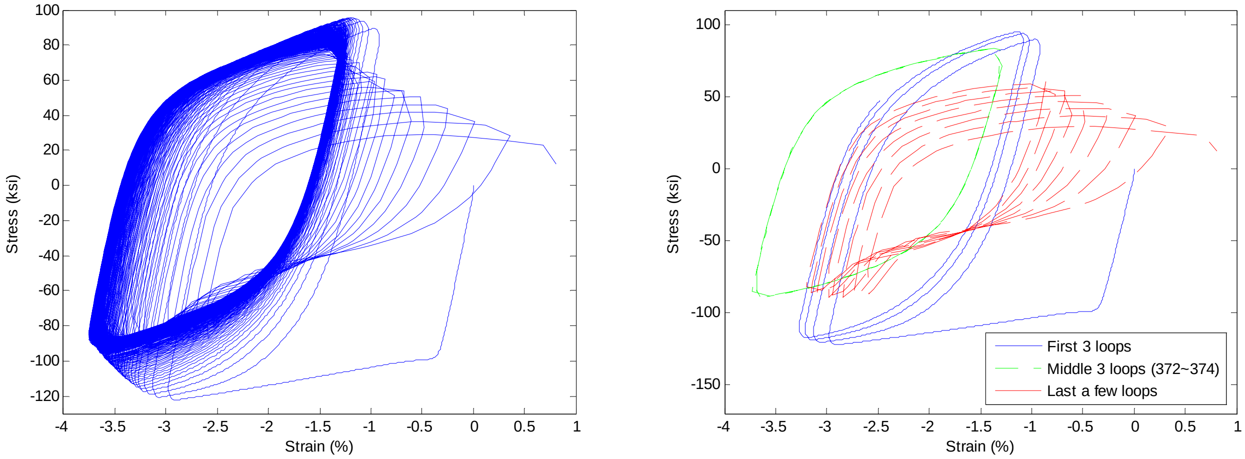

(a) (b)

Figure 3-4: Low-Cycle Fatigue Hysteresis Loops for Enduramet 32 at Strain Amplitude 1.205% (R<-1)
(a). Whole Loops (b). Loop Extract

Three complete fatigue test results and their representative loops (total strain vs. stress) for 316LN rebar, including the cases of zero mean strain ($R = -1$), positive mean strain ($R > -1$) and negative mean strain ($R < -1$), are presented in Figures 3-5, 3-6 and 3-7, respectively.

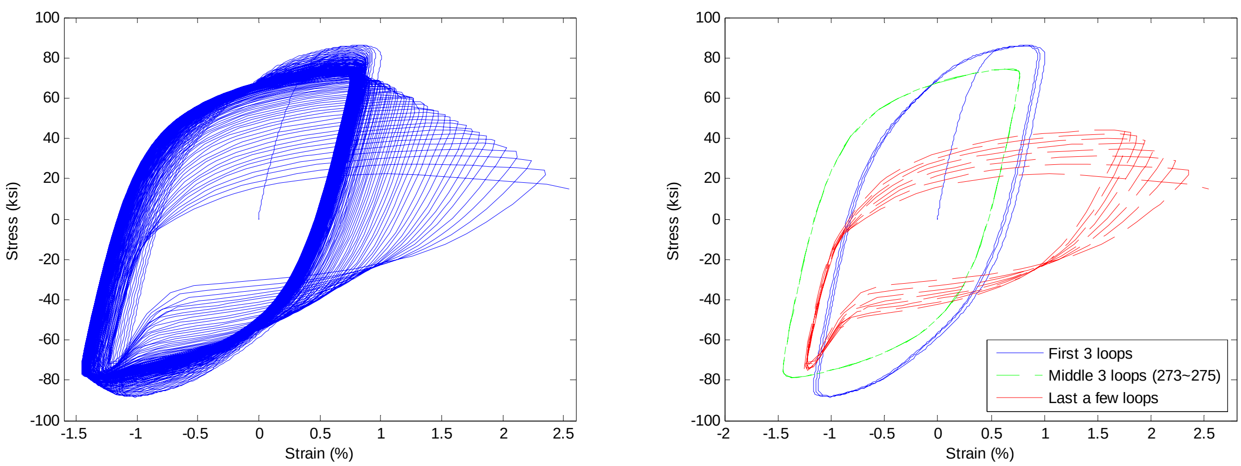

(a) (b)

Figure 3-5: Low-Cycle Fatigue Hysteresis Loops for 316LN at Strain Amplitude 1.116% (R=-1)
(a). Whole Loops (b). Loop Extract

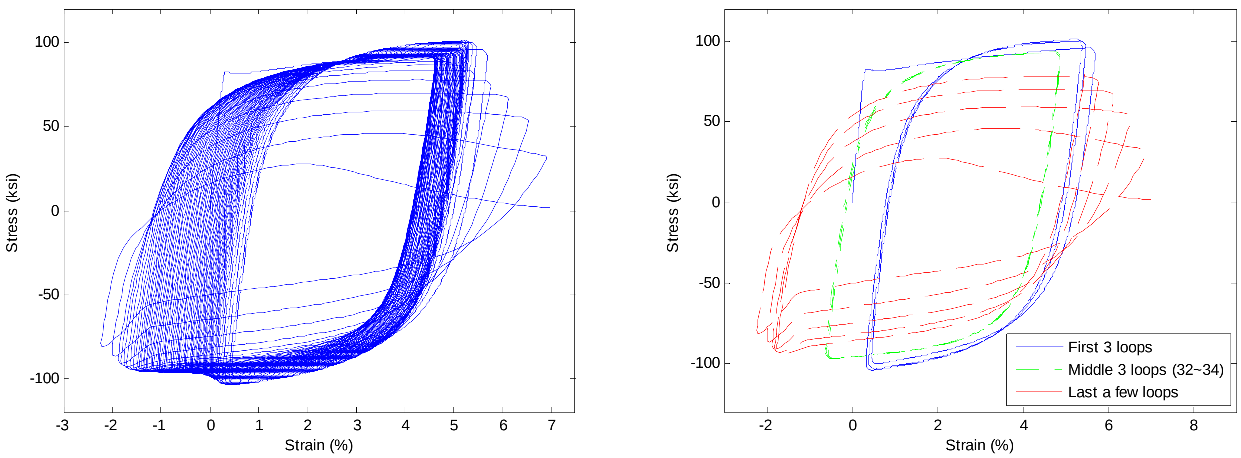

(a) (b)

Figure 3-6: Low-Cycle Fatigue Hysteresis Loops for 316LN at Strain Amplitude 2.694% (R>-1)
(a). Whole Loops (b). Loop Extract

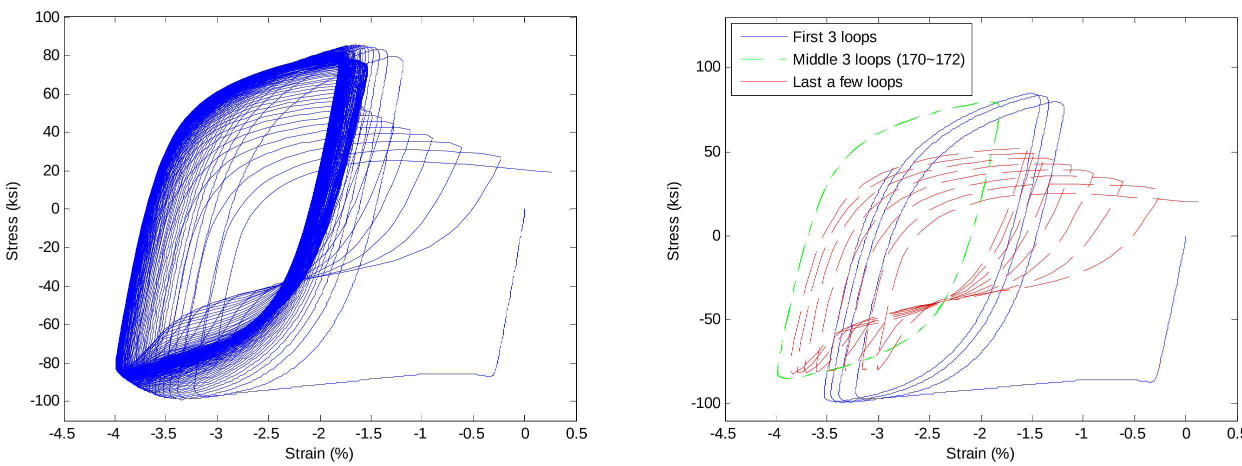

(a) (b)

Figure 3-7: Low-Cycle Fatigue Hysteresis Loops for 316LN at Strain Amplitude 1.097% (R<-1)
(a). Whole Loops (b). Loop Extract

Three complete fatigue test results and their representative loops (total strain vs. stress) for 2205 Duplex rebar, including the cases of zero mean strain ($R=-1$), positive mean strain ($R>-1$) and negative mean strain ($R<-1$), are presented in Figures 3-8, 3-9 and 3-10, respectively.

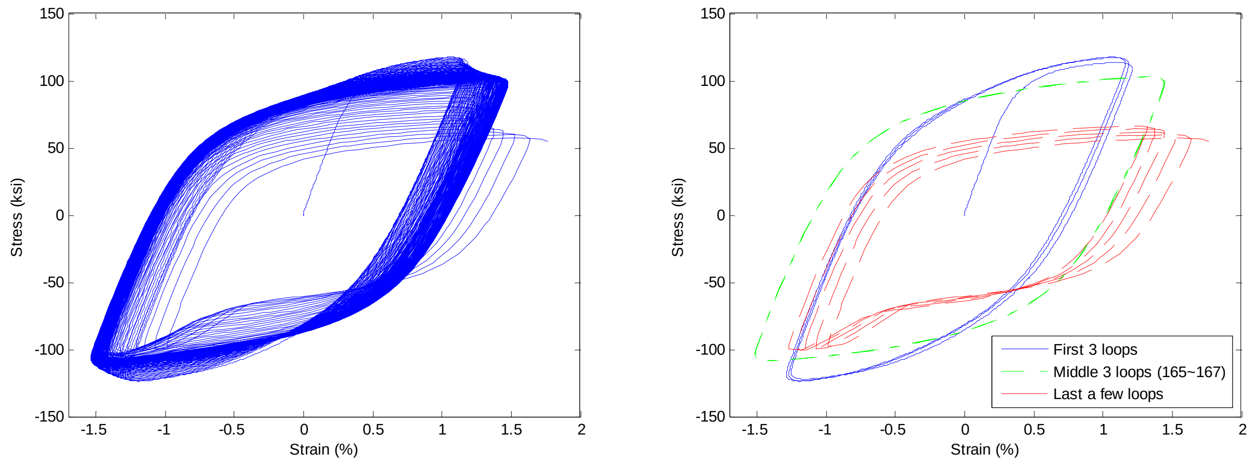

(a) (b)

Figure 3-8: Low-Cycle Fatigue Hysteresis Loops for 2205 Duplex at Strain Amplitude 1.450% (R=-1)
(a). Whole Loops (b). Loop Extract

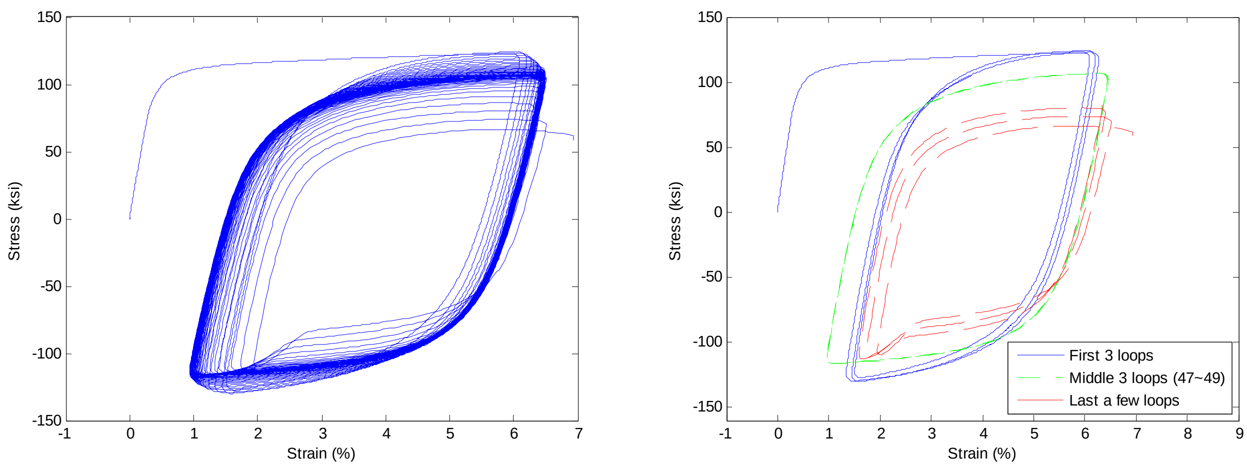

(a) (b)

Figure 3-9: Low-Cycle Fatigue Hysteresis Loops for 2205 Duplex at Strain Amplitude 2.744% (R>-1)
(a). Whole Loops (b). Loop Extract

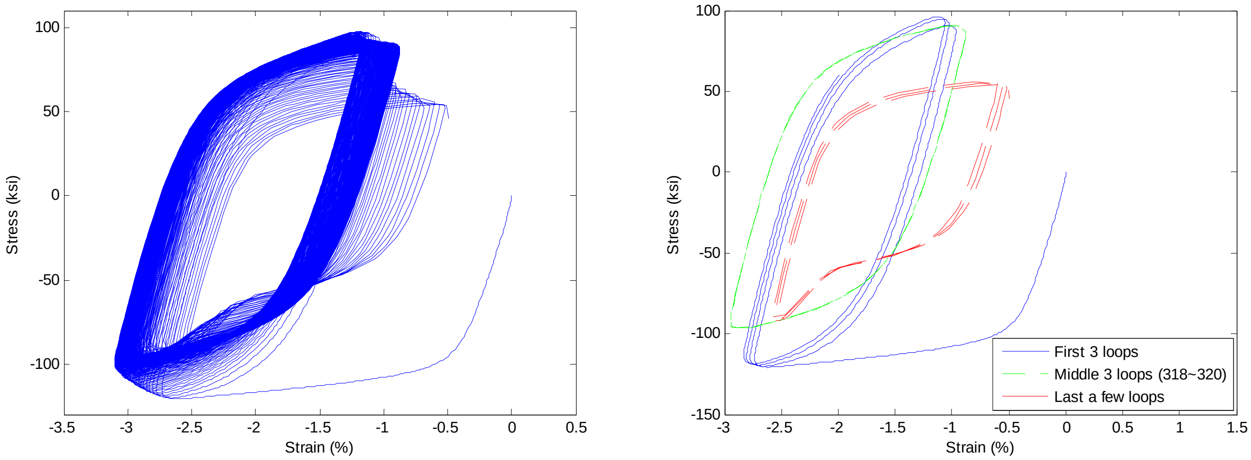

(a) (b)

Figure 3-10: Low-Cycle Fatigue Hysteresis Loops for 2205 Duplex at Strain Amplitude 1.014% (R<-1)
(a). Whole Loops (b). Loop Extract

Three complete fatigue test results and their representative loops (total strain vs. stress) for A706G60 rebar, including the cases of zero mean strain ($R = -1$), positive mean strain ($R > -1$) and negative mean strain ($R < -1$), are presented in Figures 3-11, 3-12 and 3-13, respectively.

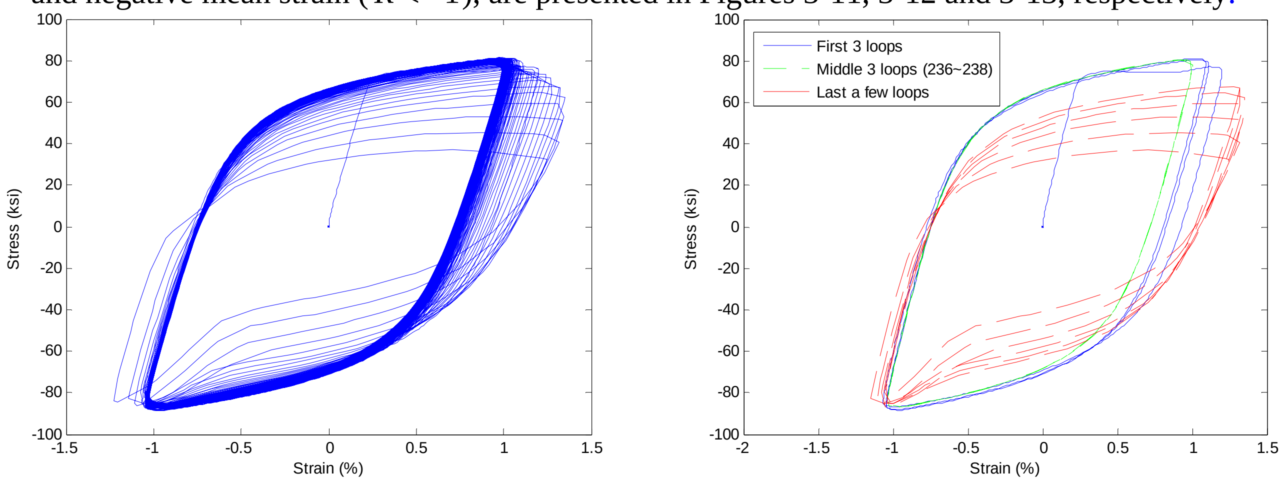

(a) (b)

Figure 3-11: Low-Cycle Fatigue Hysteresis Loops for A706G60 at Strain Amplitude 1.022% (R=-1)
(a). Whole Loops (b). Loop Extract

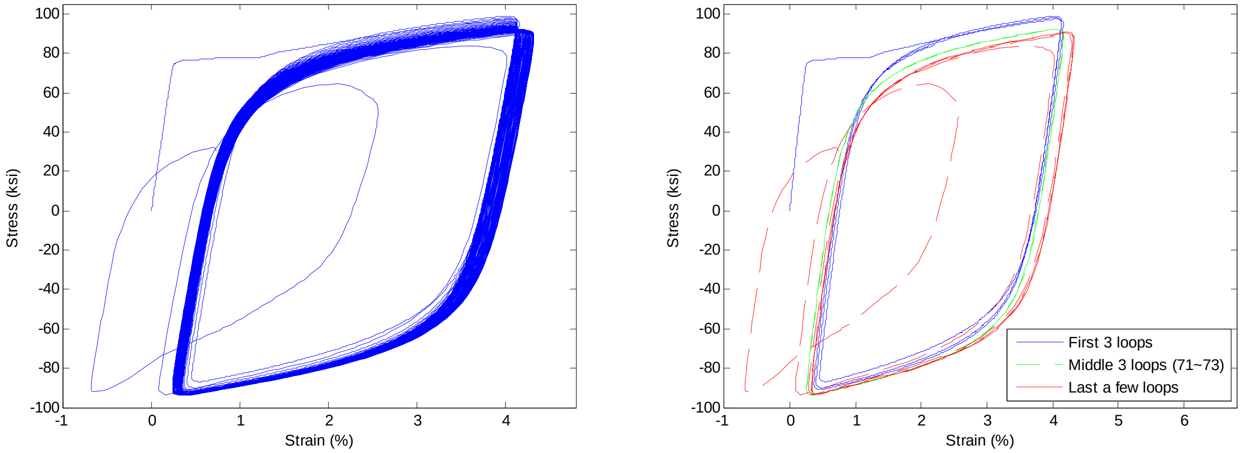

(a) (b)

Figure 3-12: Low-Cycle Fatigue Hysteresis Loops for A706G60 at Strain Amplitude 1.946% (R>-1)
(a). Whole Loops (b). Loop Extract

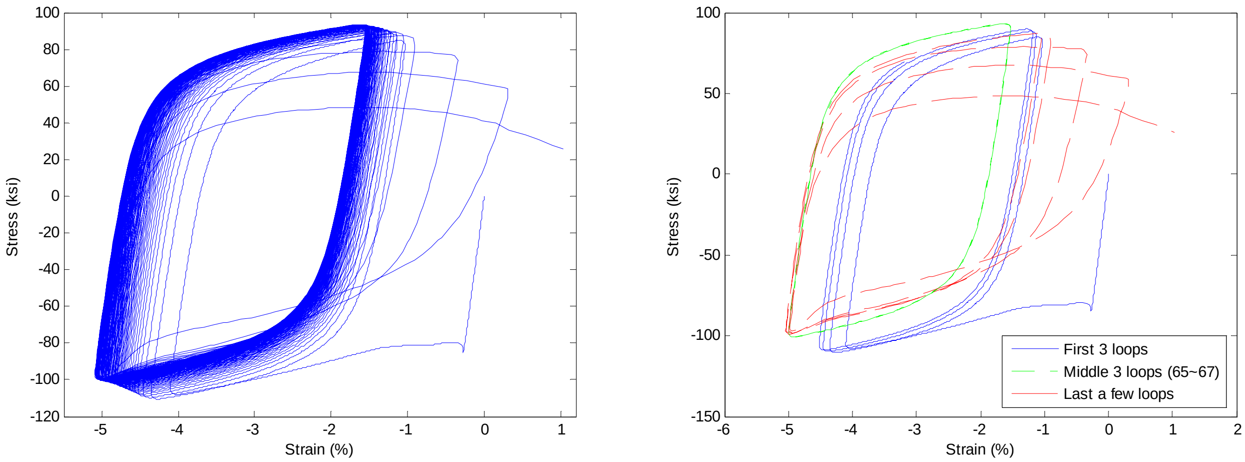

(a) (b)

Figure 3-13: Low-Cycle Fatigue Hysteresis Loops for A706G60 at Strain Amplitude 1.715% (R<-1)
(a). Whole Loops (b). Loop Extract

Three complete fatigue test results and their representative loops (total strain vs. stress) for MMFX II rebar, including the cases of zero mean strain ($R = -1$), positive mean strain ($R > -1$) and negative mean strain ($R < -1$), are presented in Figures 3-14, 3-15 and 3-16, respectively.

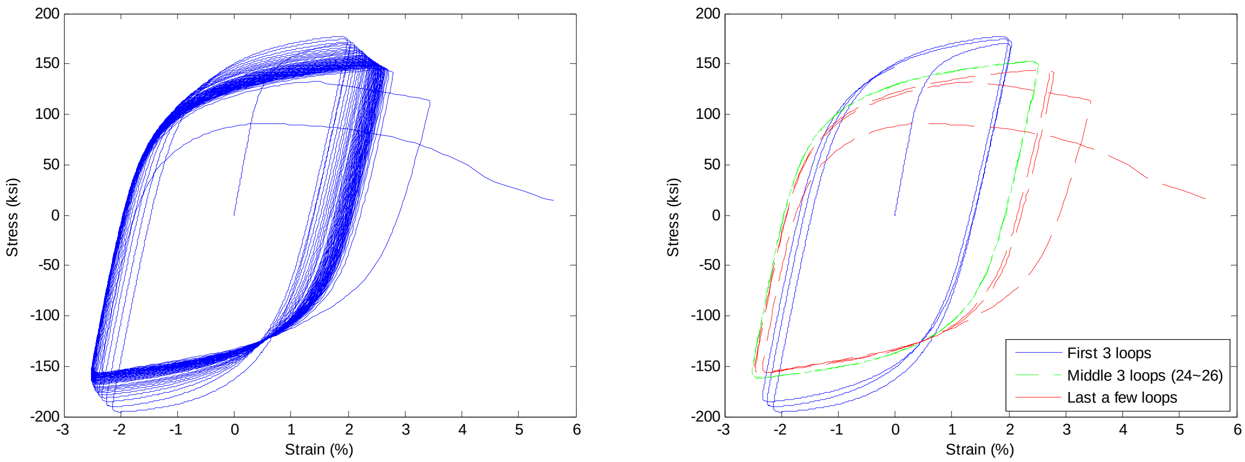

(a) (b)

Figure 3-14: Low-Cycle Fatigue Hysteresis Loops for MMFX II at Strain Amplitude 2.424% (R=-1)
(a). Whole Loops (b). Loop Extract

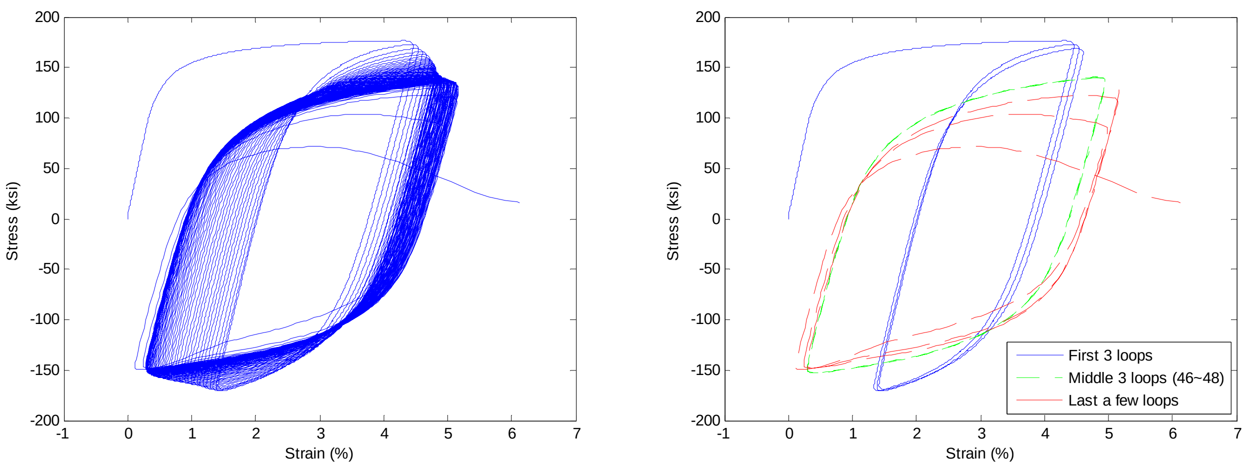

(a) (b)

Figure 3-15: Low-Cycle Fatigue Hysteresis Loops for MMFX II at Strain Amplitude 2.123% (R>-1)
(a). Whole Loops (b). Loop Extract

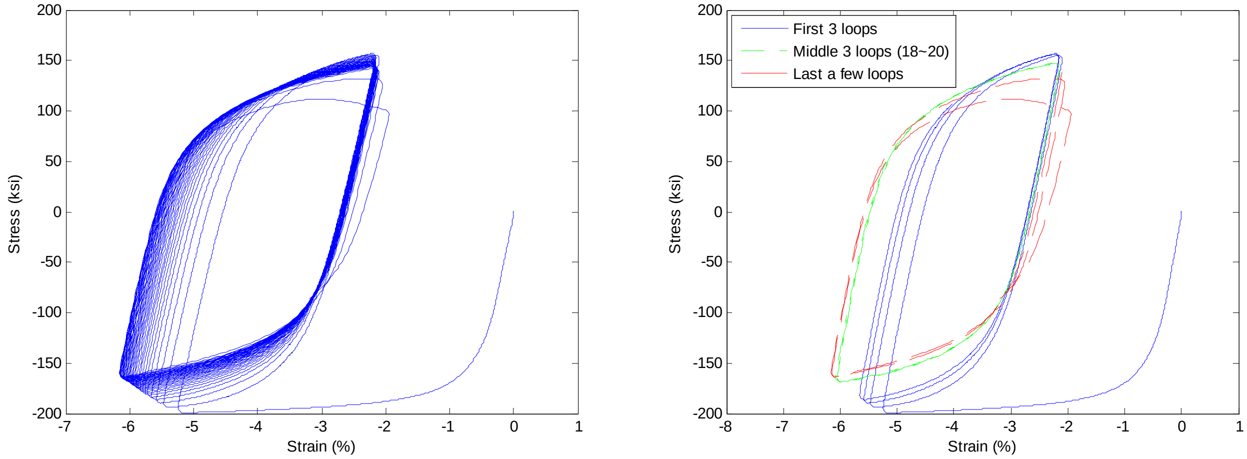

(a) (b)

Figure 3-16: Low-Cycle Fatigue Hysteresis Loops for MMFX II at Strain Amplitude 1.875% (R<-1)
(a). Whole Loops (b). Loop Extract

3.3 Test Results of Low-Cycle Fatigue Tests

Detailed experimental data for Enduramet 32, 316LN, 2205 Duplex, A706G60 and MMFX II are listed in Tables 3-2 to 3-5, respectively.

Table 3-2: Low-Cycle Fatigue Test Data for Enduramet 32

ε_a (%)	ε_p (%)	N_f	W_T (ksi)	W_m (ksi)	Mean Strain (%)
2.238	2.235	202.5	125760	597.751	-0.173
1.966	1.847	158.5	81574	516.14	0.054
2.004	1.992	243.5	117030	480.885	-0.797
1.664	1.664	433	160470	366.007	-0.038
1.574	1.566	538.5	176460	331.116	-0.378
1.654	1.558	445	150760	331.126	-0.189
1.449	1.446	508.5	155150	299.903	0.059
1.205	1.201	770.5	170510	221.697	0.141
0.932	0.930	1687	260310	150.705	-0.165
0.763	0.761	3010	335650	106.210	-0.073
3.552*	3.549*	17*	18469*	1530.7*	-----
5.121*	4.549*	11*	21862*	1916.2*	0.822*
4.550*	4.041*	31*	56590*	1905.2*	-1.046*
2.812*	2.700*	81*	64080*	729.279*	0.852*
2.608	2.481	119.5	88870	714.007	3.049
2.235	2.220	255.5	149820	576.930	2.570
1.884	1.862	247.5	115960	455.348	2.482
1.647	1.644	296.5	106750	357.421	2.430
0.990	0.987	752.5	129180	172.821	1.423
2.284	2.236	131.5	84617	640.937	-4.882
1.615	1.565	181.5	74607	400.259	-2.993
1.205	1.199	744.5	182870	246.235	-2.488

ε_a : total strain amplitude

ε_p : plastic strain amplitude

N_f : cycles of fatigue life

W_T : total loop area

W_m : mid loop area

* Data is excluded from the regression analysis due to the severe specimen buckling.

Table 3-3: Low-Cycle Fatigue Test Data for 316LN

ε_a (%)	ε_p (%)	N_f	W_T (ksi)	W_m (ksi)	Mean Strain (%)
2.375	2.372	90.5	64186	693.535	-1.571
2.008	2.005	158.5	83472	507.253	-0.769
1.715	1.712	167	68686	403.026	-0.297
1.741	1.727	203.5	83044	405.334	-0.937
1.493	1.491	219.5	71347	327.060	-0.171
1.328	1.326	229.5	67711	279.770	-0.498
1.389	1.373	368.5	114360	301.631	-0.552
1.116	1.111	546.5	112530	203.912	-0.317
0.807	0.804	1337	168240	127.346	-0.271
1.008	0.988	821.5	143570	171.839	-0.282
7.250*	-----	3*	-----	3134.78	-----
5.179*	-----	5*	-----	1914.1*	-----
3.673*	-----	7*	-----	1246*	-----
3.445*	-----	30*	-----	1147.6*	-----
2.694	2.638	65.5	52223	753.287	2.299
2.385	2.335	72.5	48921	652.080	0.801
2.052	2.050	128.5	69216	532.848	0.545
1.346	1.343	239.5	71846	308.435	0.261
1.345	1.329	282.5	79381	274.805	0.956
1.912	1.801	79.5	43019	534.745	-3.038
1.404	1.285	168.5	53314	333.806	-2.719
1.097	1.035	341.5	74455	214.542	-2.860

ε_a : total strain amplitude

ε_p : plastic strain amplitude

N_f : cycles of fatigue life

W_T : total loop area

W_m : mid loop area

* Data is excluded from the regression analysis due to the severe specimen buckling.

Table 3-4: Low-Cycle Fatigue Test Data for 2205 Duplex

ε_a (%)	ε_p (%)	N_f	W_T (ksi)	W_m (ksi)	Mean Strain (%)
2.252	2.194	148	100710	687.241	0.116
2.213	2.166	182	115220	634.086	-0.310
1.837	1.815	292	153640	509.691	-0.261
1.450	1.432	331	120600	371.559	-0.097
1.465	1.447	345	128410	367.187	-0.105
1.326	1.316	578	182290	310.949	0.019
1.228	1.218	618	169370	279.468	0.105
0.856	0.850	1250	192240	152.088	0.252
1.316	1.305	570	170890	297.374	-0.248
0.964	0.957	873	169330	195.562	-0.091
7.100*	-----	12*	-----	2519.000*	-----
4.750*	-----	21*	-----	1792.700*	-----
4.385*	-----	18*	-----	1575.500*	-----
3.433*	-----	40.5*	-----	1350.400*	-----
2.744	2.585	94.5	79345	852.032	3.770
2.096	2.032	165.5	99831	601.018	3.828
1.837	1.780	184.5	93894	505.083	3.082
1.502	1.469	275.5	102690	378.224	2.852
1.153	1.142	526.5	126140	245.294	2.358
2.257	2.167	107.5	74981	734.300	-4.262
1.587	1.553	238.5	99668	437.093	-3.323
1.014	1.006	636.5	134400	216.719	-1.992

ε_a : total strain amplitude

ε_p : plastic strain amplitude

N_f : cycles of fatigue life

W_T : total loop area

W_m : mid loop area

* Data is excluded from the regression analysis due to the severe specimen buckling.

Table 3-5: Low-Cycle Fatigue Test Data for A706G60

ε_a (%)	ε_p (%)	N_f	W_T (ksi)	W_m (ksi)	Mean Strain (%)
2.614	2.560	68	53784	750.987	-1.009
2.437	2.302	79	52870	655.889	-0.852
2.074	2.031	109	60346	537.412	-0.397
1.393	1.372	184	63332	337.472	0.058
1.407	1.391	237.5	78002	324.155	0.019
1.461	1.444	264.5	92616	341.985	-0.557
1.390	1.374	242.5	77006	309.876	-0.152
1.022	1.012	472	95522	201.602	-0.044
0.744	0.738	800	95449	123.955	-0.020
0.673	0.668	1186	119740	97.332	-0.240
7.000*	-----	2.5*	-----	-----	-----
3.524*	-----	4*	-----	1887.500*	-----
4.432*	-----	7.5*	-----	1447.700*	-----
3.666*	-----	25.5*	-----	1099.900*	-----
2.246	2.039	57.5	34474	585.035	4.158
2.253	2.143	73	43238	590.174	3.192
1.946	1.905	142.5	72000	487.814	2.220
1.550	1.516	166.5	59803	376.729	2.301
1.320	1.304	284.5	77457	267.476	0.862
2.541	2.239	42.5	32535	757.824	-4.662
1.715	1.679	130.5	60117	447.646	-3.196
1.121	1.107	323.5	80649	243.804	-2.409

ε_a : total strain amplitude
ε_p : plastic strain amplitude

N_f : cycles of fatigue life

W_T : total loop area
W_m : mid loop area

* Data is excluded from the regression analysis due to the severe specimen buckling.

Table 3-6: Low-Cycle Fatigue Test Data for MMFX II

ε_a **(%)**	ε_p **(%)**	N_f	W_T **(ksi)**	W_m **(ksi)**	**Mean Strain (%)**
2.554	2.317	44	50845	1166.800	0.330
2.424	2.200	49	51931	1024.900	-0.061
2.117	1.921	55	45961	885.076	0.247
1.761	1.633	70	47147	669.311	-0.220
1.606	1.555	142	77888	558.453	0.015
1.385	1.255	166	86834	527.012	-0.155
1.386	1.341	187	84525	464.776	-0.098
1.279	1.238	261	107130	419.569	-0.089
1.172	1.145	236	79711	352.773	-0.125
1.159	1.121	396	125400	331.671	0.077
7.500*	-----	4*	-----	-----	-----
6.750*	-----	5*	-----	-----	-----
6.502*	-----	6*	-----	6917.300*	-----
4.231*	-----	12*	-----	2120.900*	-----
2.673	2.373	25	43892	1061.800	4.785
2.123	1.926	93.5	76621	834.934	2.747
2.054	1.971	105	73065	700.657	4.077
1.305	1.281	290.5	107960	379.760	2.806
1.005	0.963	643	126730	210.170	2.386
1.875	1.558	37.5	27264	716.653	-4.038
1.465	1.399	122.5	55520	463.477	-3.426
0.812	0.800	586	96644	181.195	-2.489

ε_a : total strain amplitude

ε_p : plastic strain amplitude

N_f : cycles of fatigue life

W_T : total loop area

W_m : mid loop area

* Data is excluded from the regression analysis due to the severe specimen buckling.

3.4 Data Regression

The equations below were regressed based on the first ten sets of data with mean strains of zero in Tables 3-2 to 3-6 for each type of steel, respectively. Equation (3-1) relates the plastic strain (%) (ε_p) to the fatigue life (N_f).

Enduramet 32 rebar: $$\varepsilon_p = 47(2N_f)^{-0.5} \quad \text{(3-1 a)}$$

316LN rebar: $$\varepsilon_p = 36(2N_f)^{-0.5} \quad \text{(3-1 b)}$$

2205 duplex rebar: $$\varepsilon_p = 41(2N_f)^{-0.5} \quad \text{(3-1 c)}$$

A706 G60 rebar: $$\varepsilon_p = 30(2N_f)^{-0.5} \quad \text{(3-1 d)}$$

MMFX II rebar: $$\varepsilon_p = 24(2N_f)^{-0.5} \quad \text{(3-1 e)}$$

Equation (3-3) was proposed by Mander et al. (1994) and is applicable to A615 grade 40 ordinary deformed-steel rebar and A722 high-strength prestressing thread bars. By comparing equation (3-2) to equations (3-1a), (3-1b), (3-1c), (3-1d) and (3-1e), it is found that equation (3-2) is too conservative for the five types of rebar tested. Because for a given value of N_f, equation (3-2) gives a much smaller ε_p, in other words, for a certain plastic strain amplitude (ε_p), equation (3-2) predicts a much shorter fatigue life (N_f), which would overly underestimate the service life of the stainless steel rebar.

$$\varepsilon_p = 8(2N_f)^{-0.5} \quad \text{(3-2)}$$

Figures 3-17(a) to 3-17(e) are plastic strain vs. reversal fatigue life for Enduramet 32 rebar, 316LN rebar, 2205 duplex rebar, A706G60 rebar, and MMFX II rebar, respectively.

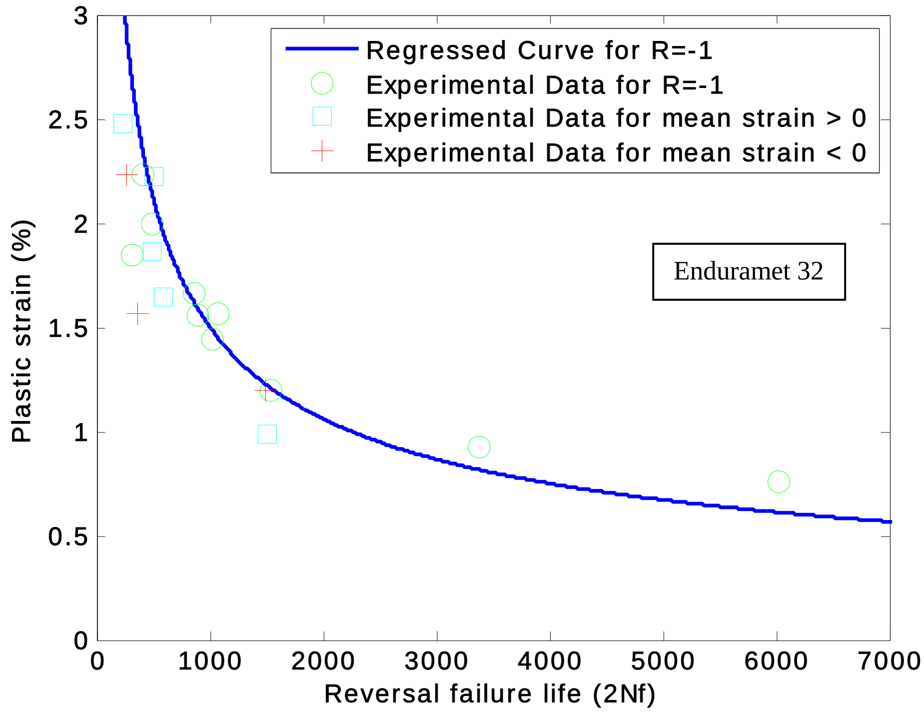

(a) Enduramet 32

Figure 3-17: Plastic Strain vs. Fatigue Life

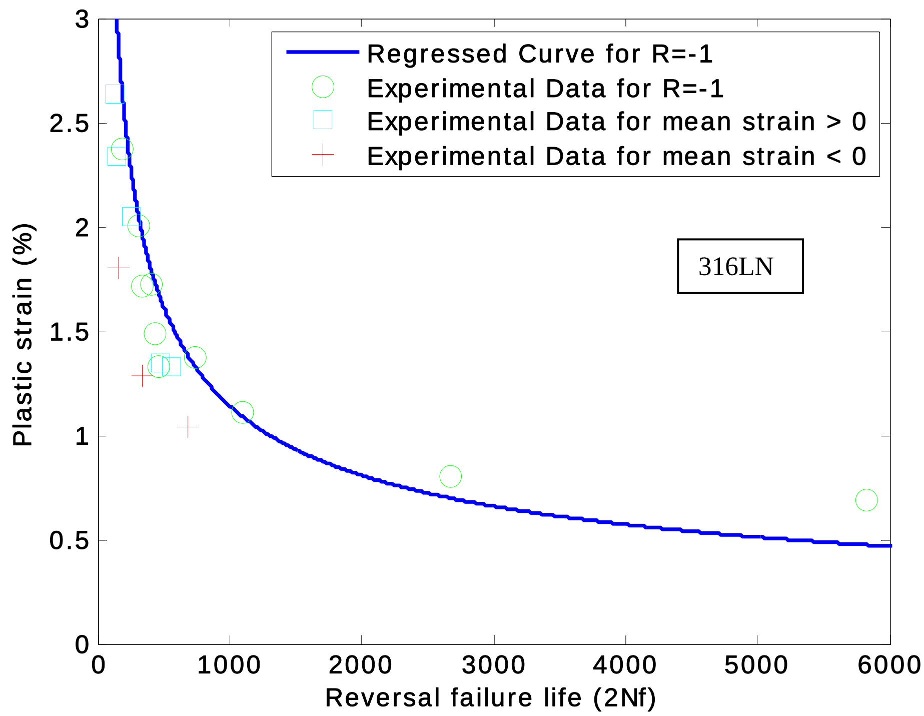

(b) 316LN

Figure 3-17: Plastic Strain vs. Fatigue Life (cont'd)

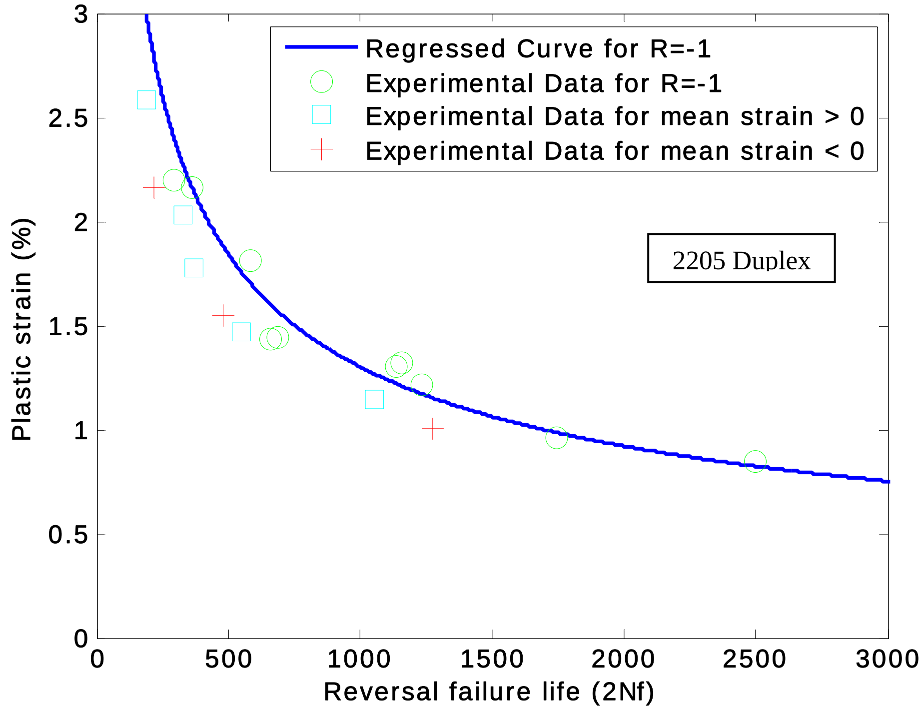

(c) 2205 Duplex

Figure 3-17: Plastic Strain vs. Fatigue Life (cont'd)

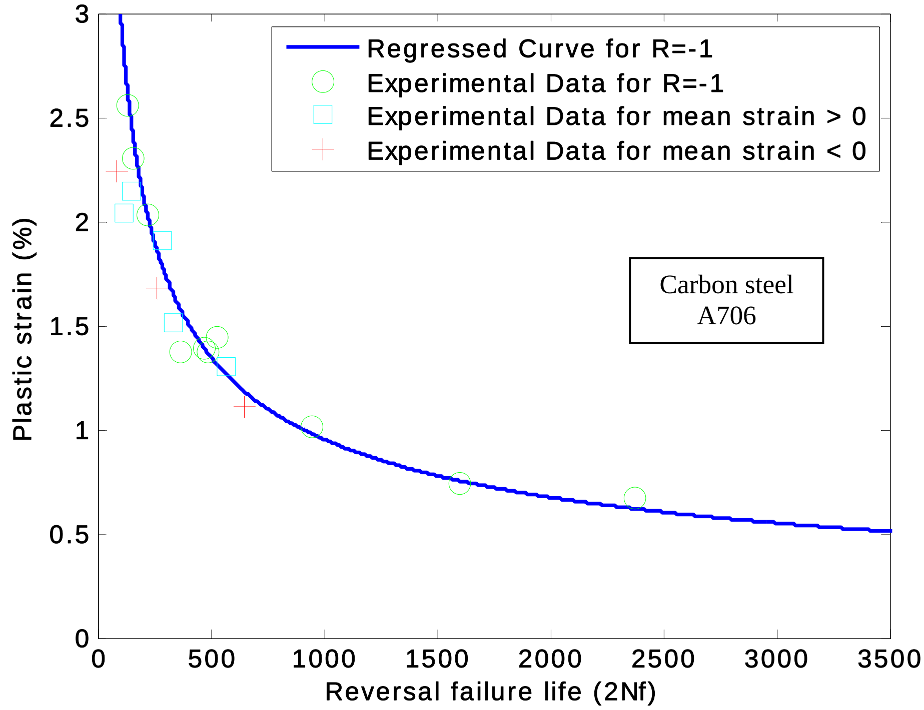

(d) A706

Figure 3-17: Plastic Strain vs. Fatigue Life (cont'd)

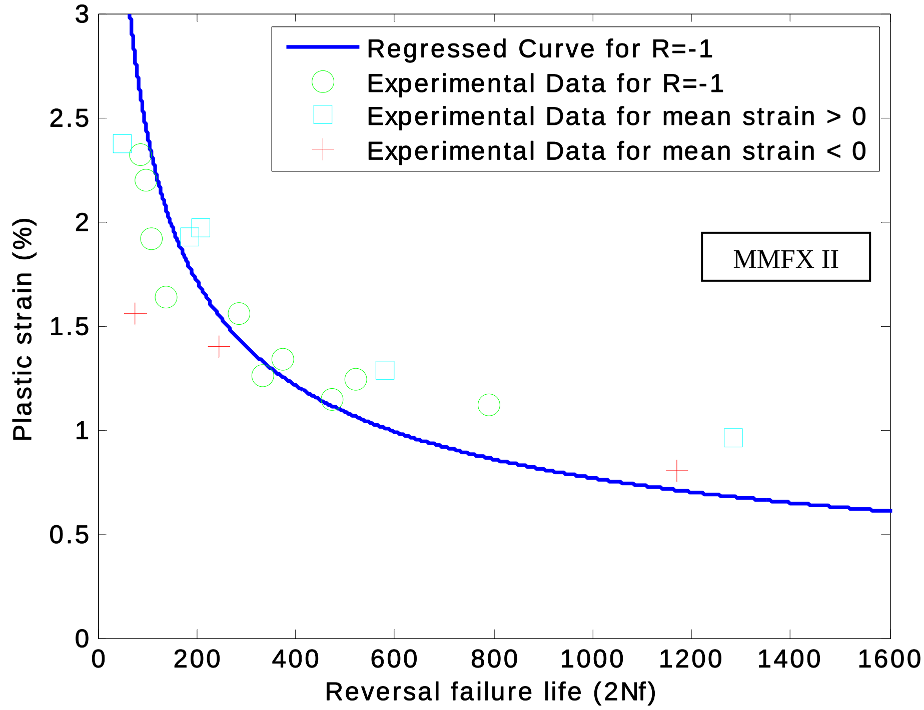

(e) MMFX II

Figure 3-17: Plastic Strain vs. Fatigue Life (cont'd)

As seen in Figure 3-17, the regressed power function relationships closely fit the experimental data, and mean strain has little effect on the fatigue life; hence mean strain effects could be ignored in the engineering application.

For the five types of steel rebar tested, regression curves for plastic strain vs. reversal fatigue life are shown in Figures 3-18.

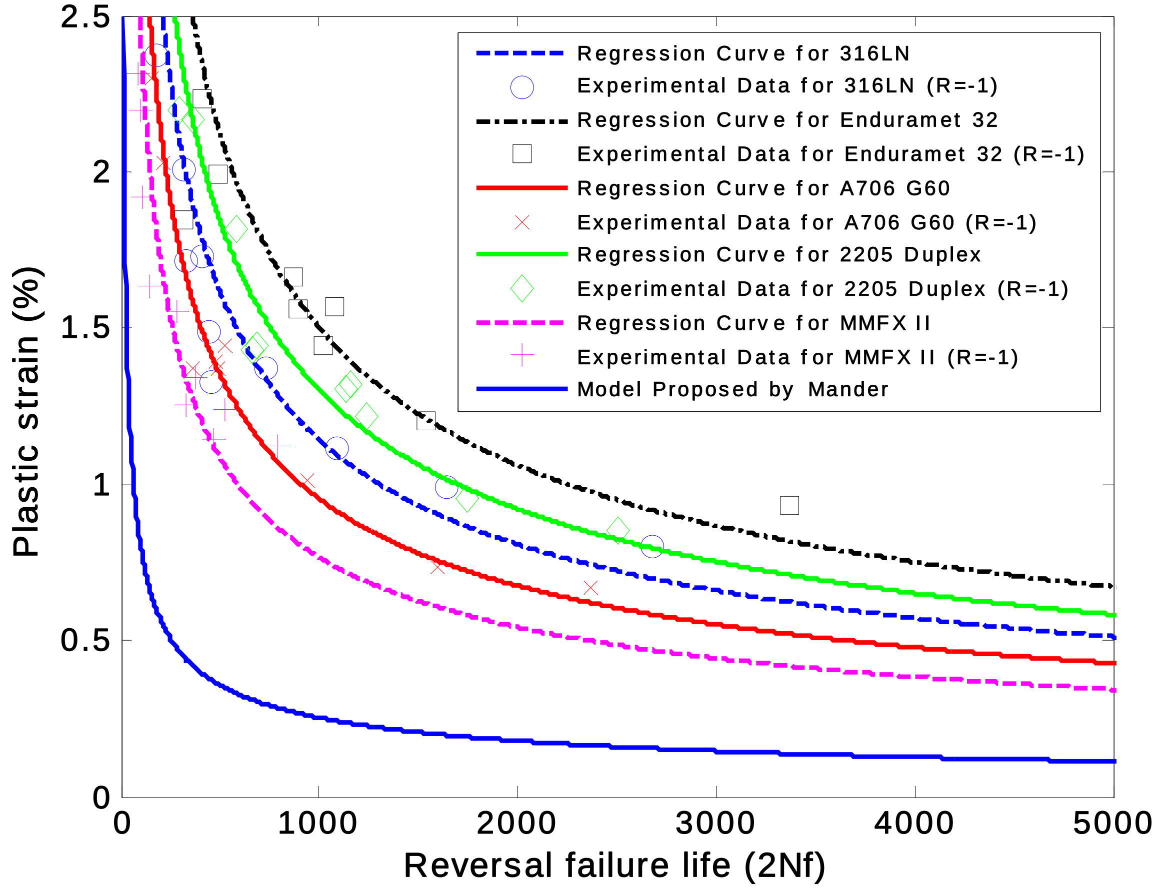

Figure 3-18: Regression Curves for Plastic Strain vs. Fatigue Life

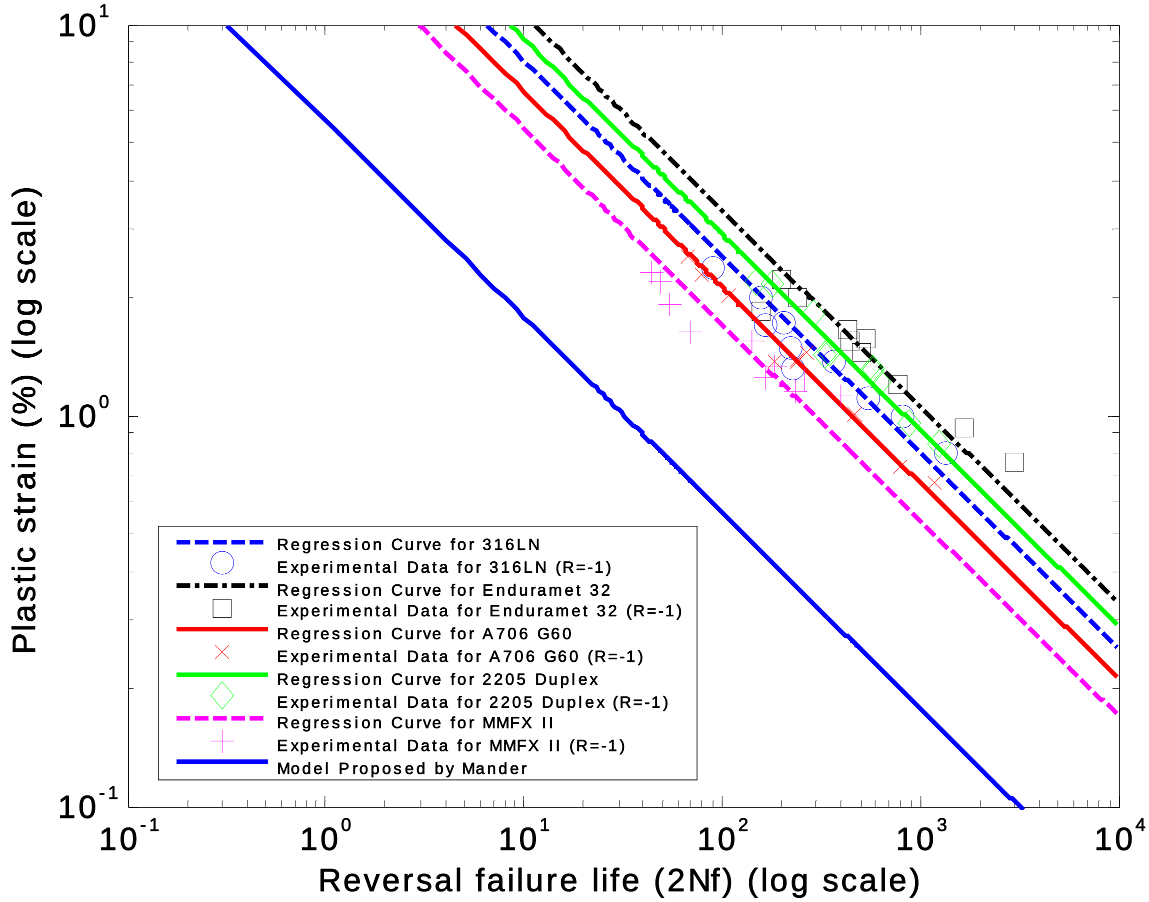

Figure 3-19: Regression Curves for Plastic Strain vs. Fatigue Life (Log Scale)

As to fatigue life prediction, if one uses equation (3-1) shown in figures 3-18 and 3-19, Enduramet 32 stainless has the longest fatigue life followed by 2205 duplex stainless, 316LN stainless, A706 G60 Carbon and MMFX II.

Based upon the discussions above, Enduramet 32 has the highest ductility and the best low-cycle fatigue performance among the steels investigated. In general, the three types of stainless steel are better than A706 G60.

3.5 Limitations of Coupon Test Results

The coupon tests provide a basic understanding of the different steel materials under earthquake loading but there are limitations to application of these exponential relationships to use in actual earthquake engineering applications. For example:

- The load frame for low-cycle fatigue test can only be controlled using prescribed strain history. When failure of the specimens was imminent, the specimens were usually distorted, changing the gauge length. That is the reason why the hysteresis loops obtained have the shifting at the strain amplitudes for the last few cycles of each specimen.

- The low-cycle fatigue tests were conducted on the individual steel rebar specimens under uni-axial strains, while the steel rebar in the real engineering applications may be subjected to multi-axial strains. This could result in a different type of behavior.

- Strain loadings induced by earthquakes are much more irregular than the complete reverse cyclic strains used for coupon tests. This irregular loading history could affect the fatigue life.

- The regressed power function relationships for different steels provided an estimate of fatigue life for a wide range of plastic strains, however, the experimental data is for a limited range of strain amplitudes. For example, large strain amplitudes, (i.e. beyond 3%), buckling of the specimen was unavoidable. This would have a strong influence on the fatigue life.

3.6 Summary and Conclusions for the Monotonic Tension Test and Constant Amplitude Low-Cycle Fatigue Test

Test results show that, compared to carbon steel, the Young's modulus (E) of the three types of stainless steel rebar are slightly smaller, and slightly higher for MMFX II. The values of E of Enduramet 32 rebar, 316 LN rebar, 2205 duplex rebar and MMFX II rebar are 98.7%, 95.8%, 91.6% and 104.3% that of A706 G60 rebar, respectively. According to the latest ACI 318 code (ACI, 2005), reinforcement in members resisting earthquake-induced forces should have values of σ_u / σ_{y2} no less than 1.25. Furthermore, the actual yield strength should exceed the specified yield strength no more than 18 ksi. Enduramet 32 rebar, 316LN rebar, 2205 duplex rebar and MMFX II rebar all meet these requirements. Among the five types of steel tested, MMFX II has the highest yielding stress $\sigma_{y2} = 100.73 ksi$. Although the use of rebar of higher yield strength may reduce structural member sizes, it tends to increase crack widths and deflections under service loads, causing problems of serviceability. Under monotonic loading, the elongations at fracture of the three types of stainless steel rebar are substantially higher than A706 G60 rebar and MMFX II rebar. Except the stainless steels, the elongation of A706 G60 (26.5%) is also higher than that of MMFX II (17.51%). This shows that the stainless steel rebar is much more ductile than A706 G60 and MMFX II, and MMFX II is least capable of elongating among the steels tested.

As seen in Figure 3-17, mean strain has little effect on the fatigue life and hence mean strain effects could be ignored in the engineering application. Equation (3-2) is too conservative in estimating the fatigue life for Enduramet 32, 316LN, and 2205 duplex stainless steels, A706 G60 rebar and MMFX II rebar as shown in equation (3-1).

If one uses equation (3-1) shown in figures 3-18 and 3-19 to predict the fatigue life, Enduramet 32 stainless has the longest fatigue life followed by 2205 duplex stainless, 316LN stainless, A706 G60 Carbon and MMFX II.

Based upon the discussions above, Enduramet 32 has the highest ductility and the best low-cycle fatigue performance among the steels investigated. In general, the three types of stainless steel are better than A706 G60.

3.7 Future Research Work

In the future research, a random loading will be applied to the steel specimens to simulate the behavior of the rebar under a load more representative of a real earthquake.

In the low-cycle fatigue test, some fracture sections are almost perpendicular to the longitudinal direction of the specimens, while the others are oblique. This shows that the shear lips do affect the growth of the crack, and further study about the influence of the shear lips on the crack growth should be studied.

Higher ductility, better low-cycle fatigue performance and lower life-cycle costs indicate that stainless steel may be applicable as energy dissipation components in precast concrete bridges used for accelerated bridge construction. This specific application deserves further study. Detailed design guidelines, such as the requirements for the development length, lap splice and confinement, will require further investigation. The comparison of the test methodologies between the machined specimens used in this experiment and the raw rebar specimens should also be developed in the future research.

CHAPTER 4
MICRO & MACRO FATIGUE PROPERTIES

4.1 Fatigue Characteristics

Fatigue failures are often called “brittle failures”. And “typical” fatigue failure exhibits the following common features:

1. Distinct crack nucleation site or sites.
2. Beach marks indicative of crack growth.
3. Distinct final fracture region.

Beach mark is one of the representative characteristics of fatigue. The term has arisen because of the similarity of the fracture pattern to sand markings left after a wave of water leaves a sandy beach. Metals are crystalline in nature, which means that atoms are arranged in an ordered manner. Most structural metals are polycrystalline and thus consist of a large number of individual ordered crystals or grains. Each grain has its own particular mechanical properties, ordering direction, and directional properties. Some grains are oriented such that planes of easy slip or glide (dislocation movement) are in the direction of the maximum applied shear stress. The onset of slip creates an appearance of one or more planes within a grain sliding relative to each other. Slip occurs under both monotonic and cyclic loading and is the localization of plastic strain (Stephens et al., 2001). A combination of fine grains on the surface and coarse grain in the bulk exhibits best fatigue lives under load controlled high cycle conditions. The typical electron microscope pictures of the fracture surfaces are illustrated below.

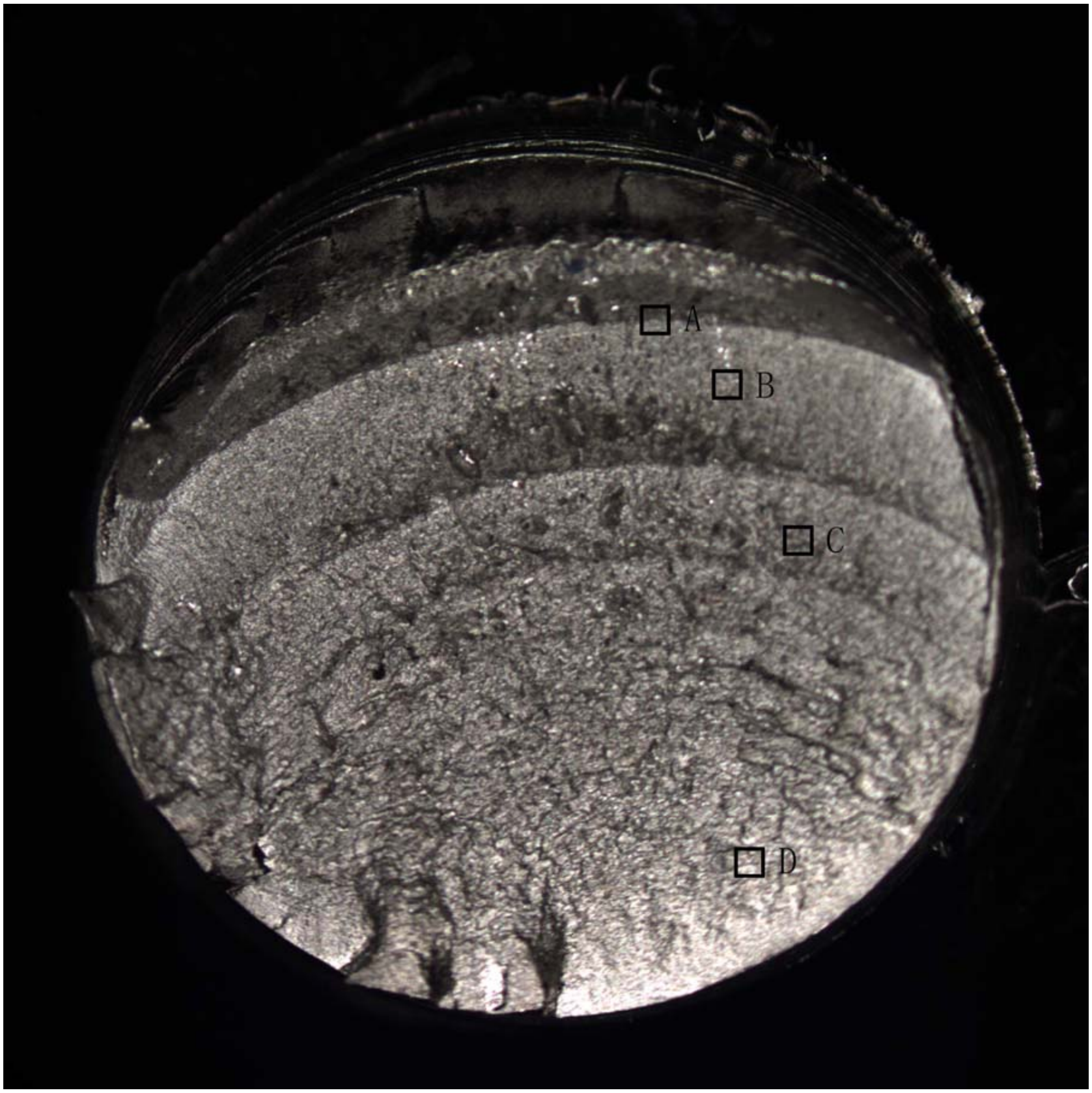

Figure 4-1: Fracture Section of Enduramet 32 at Strain Amplitude 2.238% (R = -1)

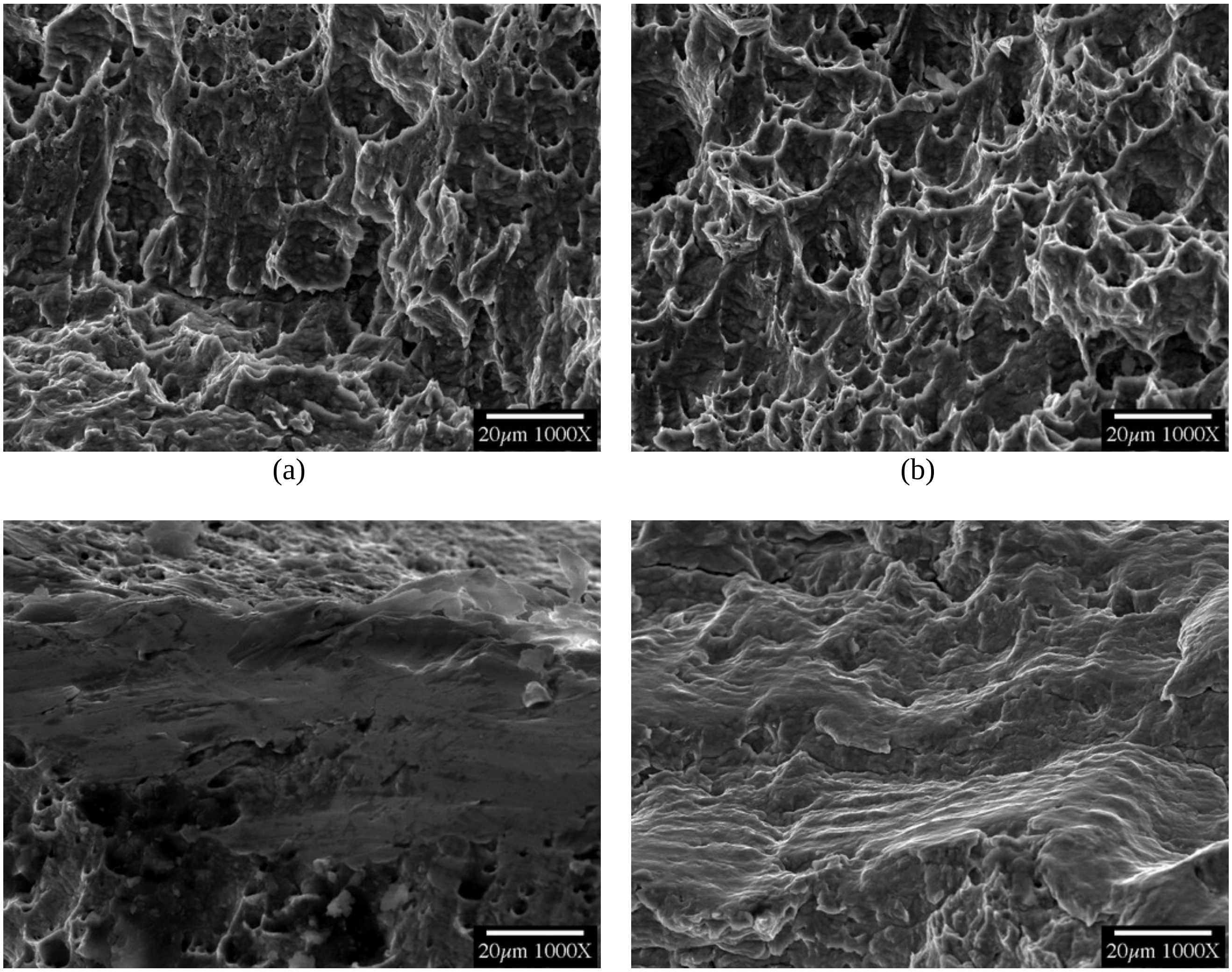

(a) (b)

(c) (d)

Figure 4-2: Electron Microscope Pictures for Fracture Section of Enduramet 32 at Strain Amplitude 2.238% (R = -1)

(a). Zoomed in Area A in Figure 4-1
(b). Zoomed in Area B in Figure 4-1
(c). Zoomed in Area C in Figure 4-1
(d). Zoomed in Area D in Figure 4-1

Figure 4-3: Fracture Section of 316LN at Strain Amplitude 2.008% (R = -1)

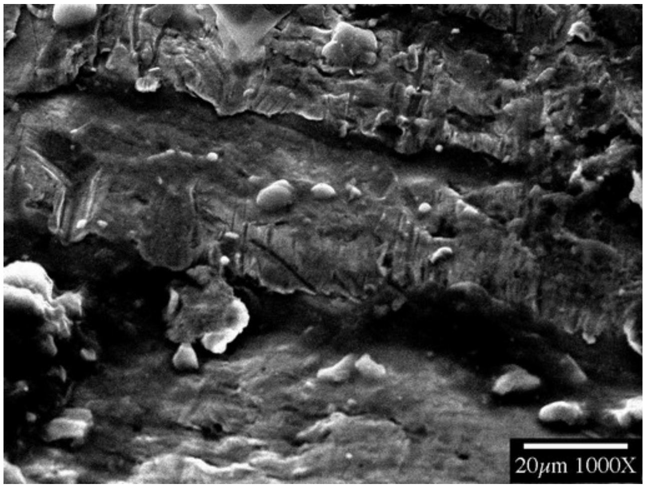

(a)

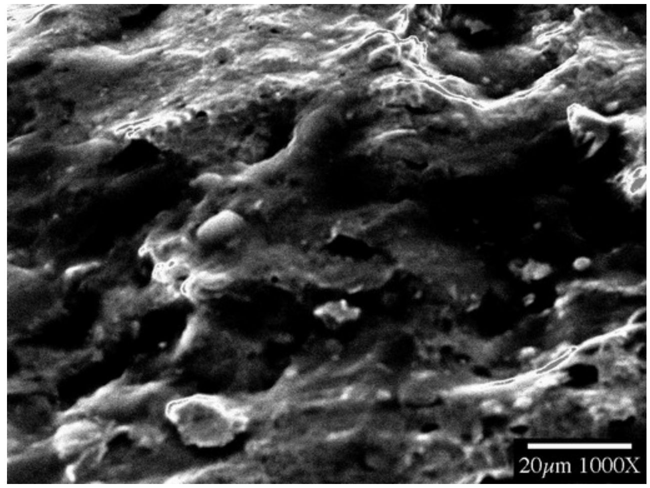

(b)

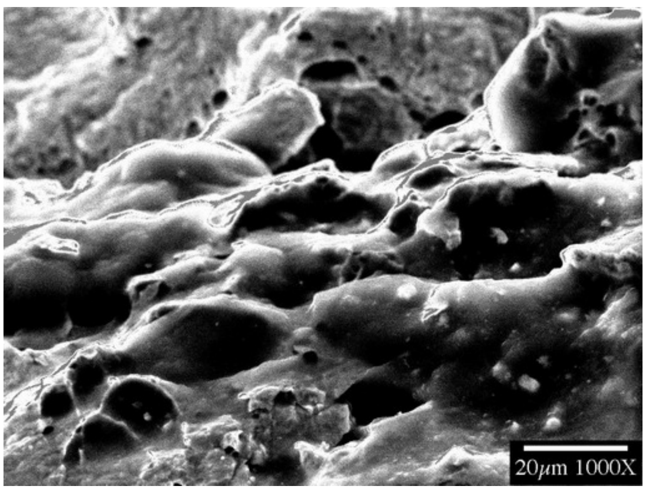

(c)

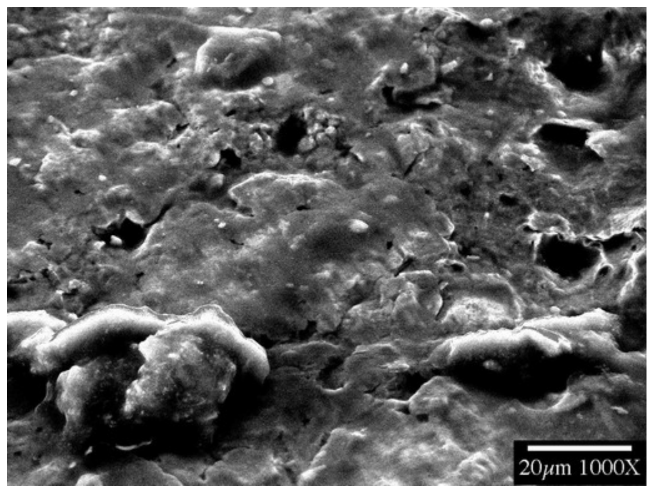

(d)

Figure 4-4: Electron Microscope Pictures for Fracture Section of 316LN at Strain Amplitude 2.008% (R = -1)
(a). Zoomed in Area A in Figure 4-3
(b). Zoomed in Area B in Figure 4-3
(c). Zoomed in Area C in Figure 4-3
(d). Zoomed in Area D in Figure 4-3

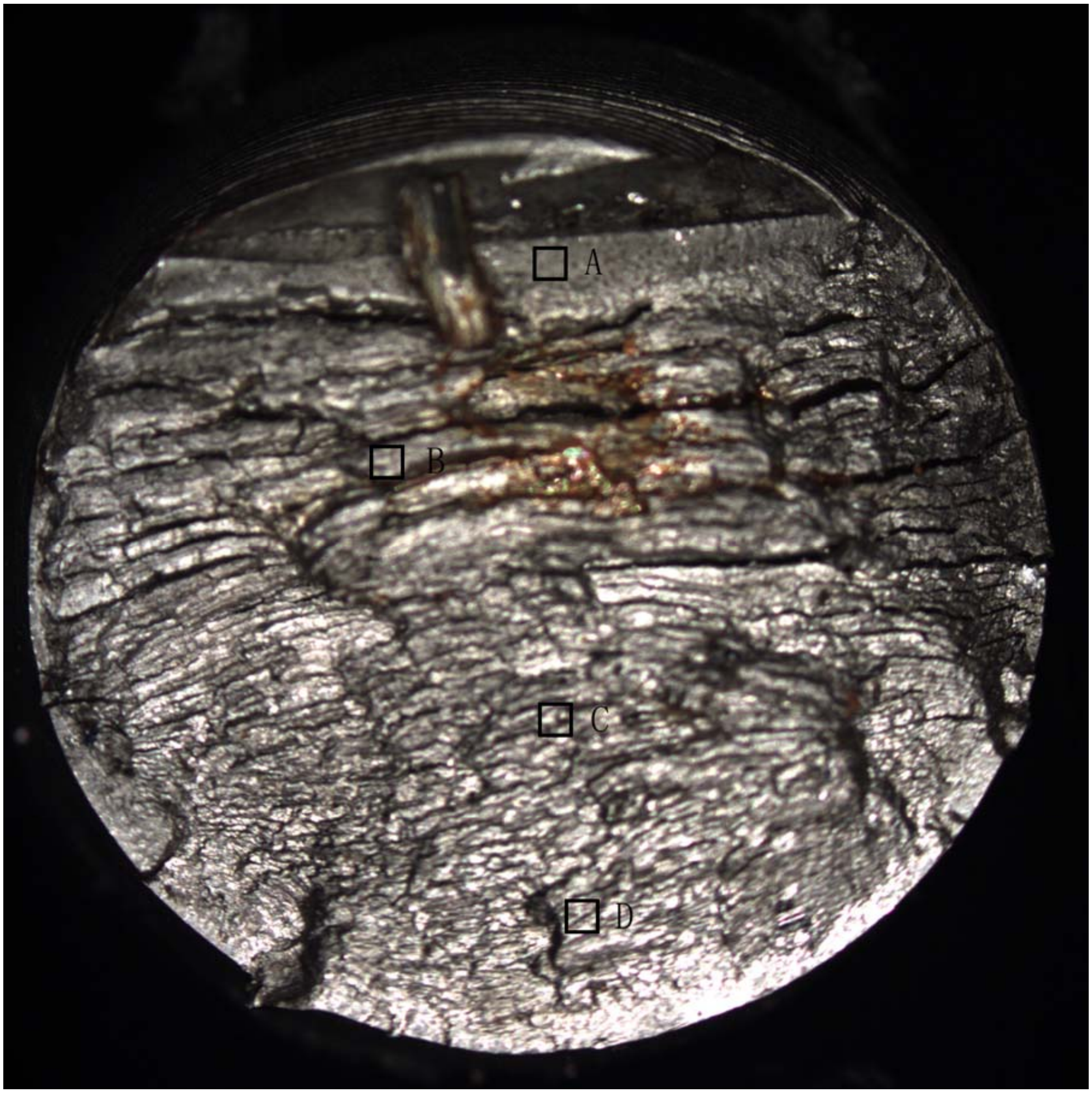

Figure 4-5: Fracture Section of 2205 Duplex at Strain Amplitude 1.837% (R = -1)

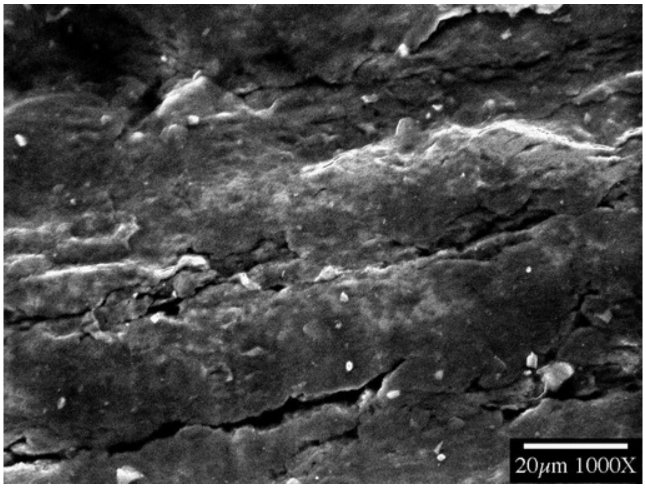

(a)

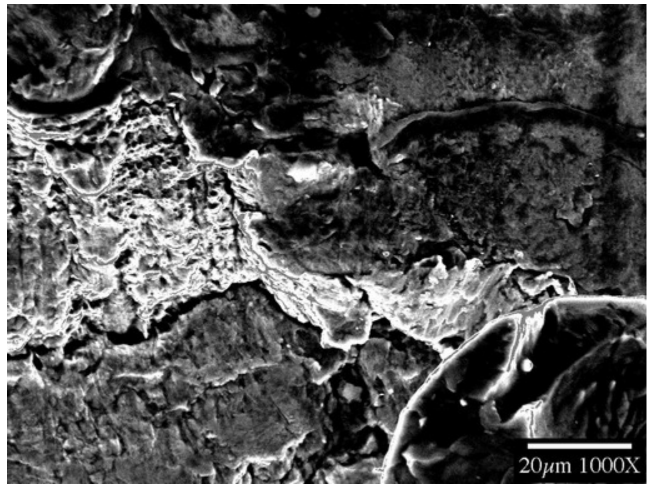

(b)

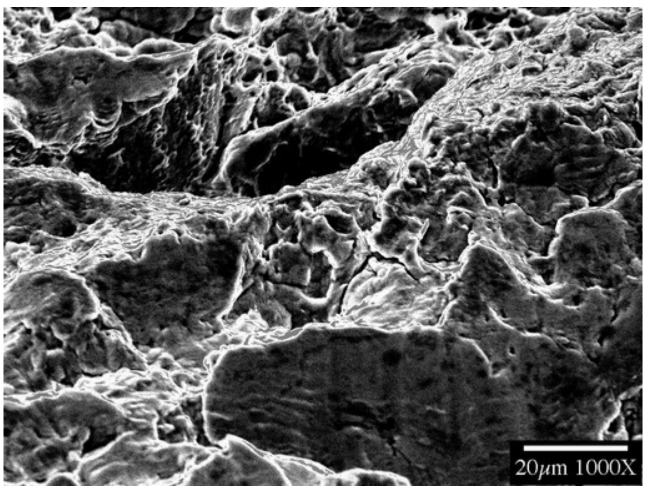

(c)

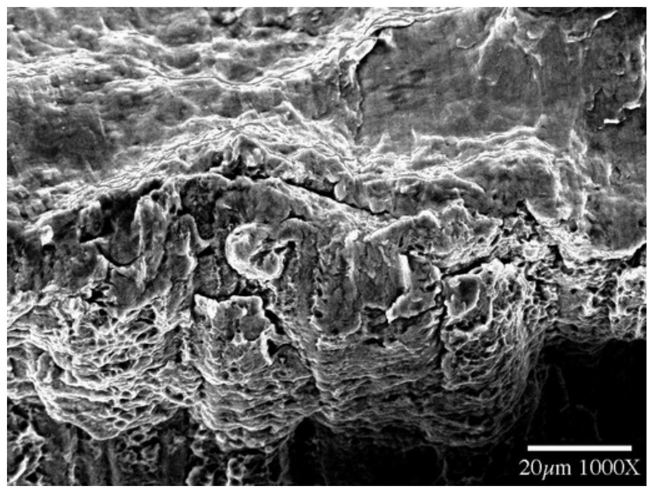

(d)

Figure 4-6: Electron Microscope Pictures for Fracture Section of 2205 Duplex at Strain Amplitude 1.837% (R = -1)
(a). Zoomed in Area A in Figure 4-5
(b). Zoomed in Area B in Figure 4-5
(c). Zoomed in Area C in Figure 4-5
(d). Zoomed in Area D in Figure 4-5

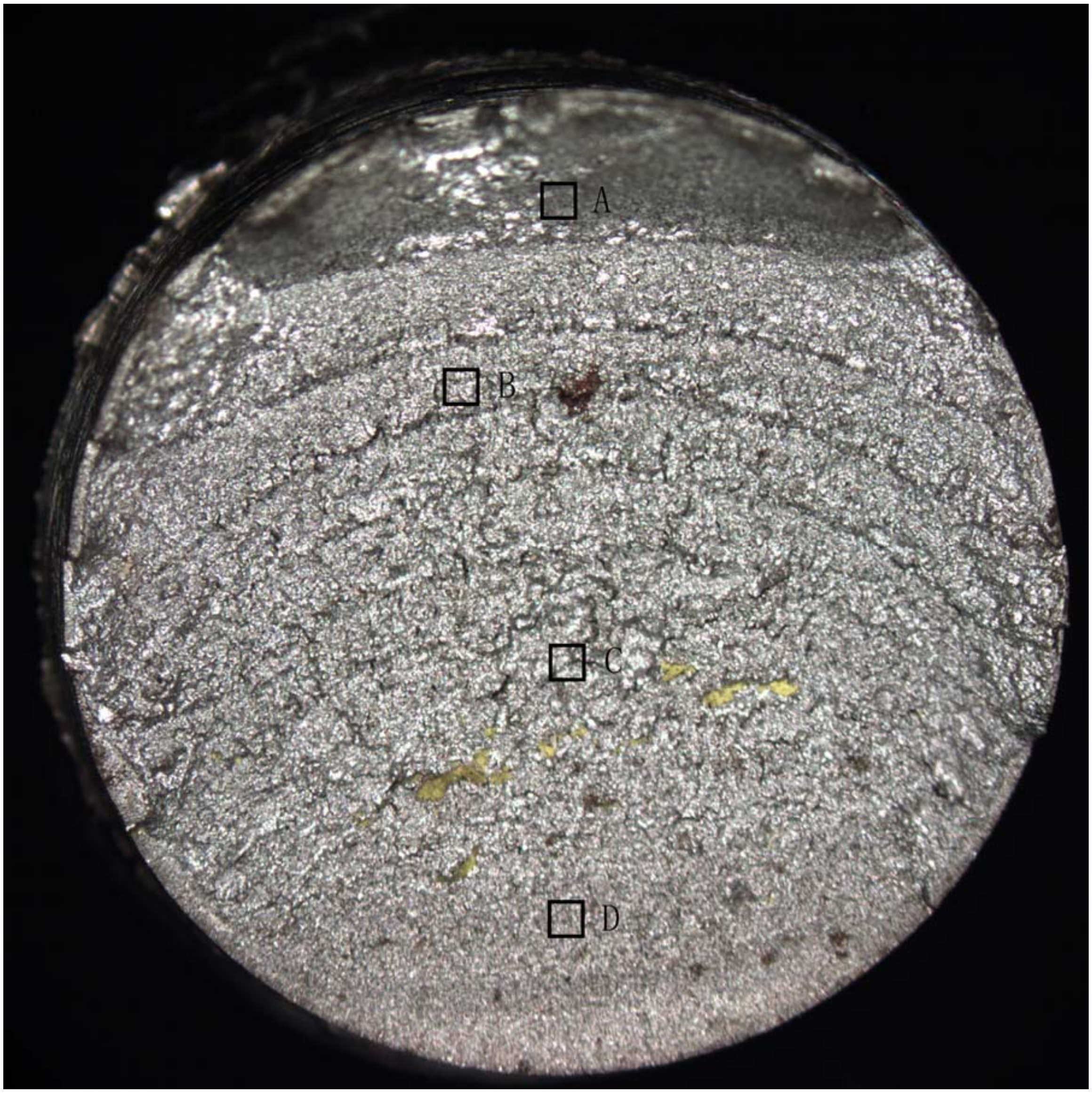

Figure 4-7: Fracture Section of A706 G60 at Strain Amplitude 1.022% (R = -1)

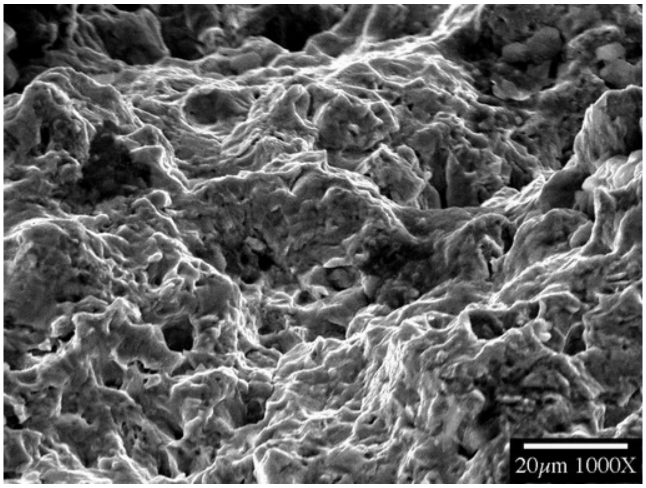

(a)

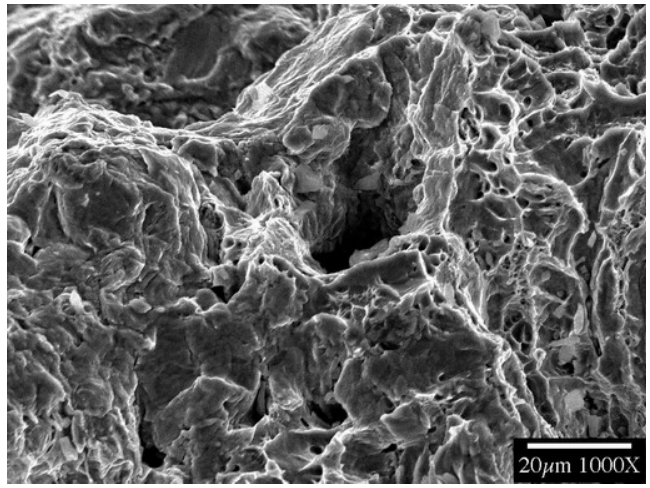

(b)

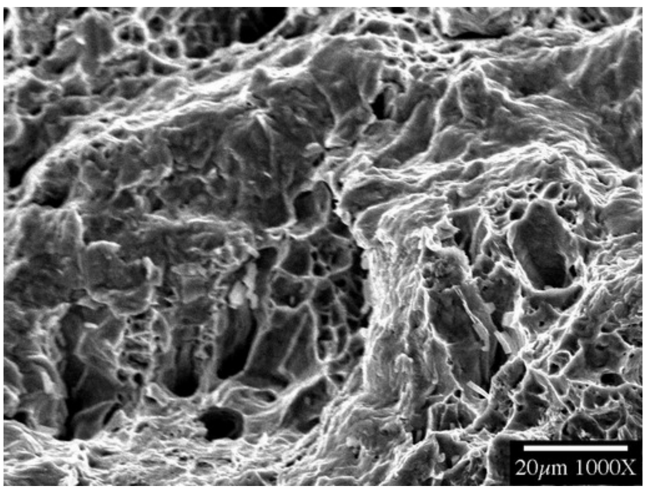

(c)

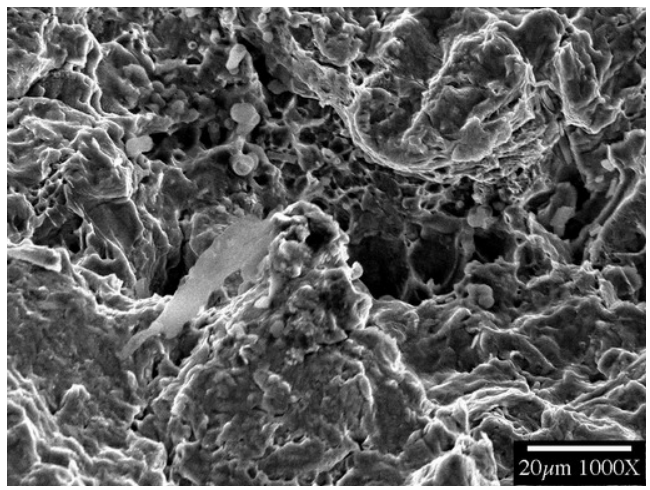

(d)

Figure 4-8: Electron Microscope Pictures for Fracture Section of A706 G60 at Strain Amplitude 1.022% (R = -1)
(a). Zoomed in Area A in Figure 4-7
(b). Zoomed in Area B in Figure 4-7
(c). Zoomed in Area C in Figure 4-7
(d). Zoomed in Area D in Figure 4-7

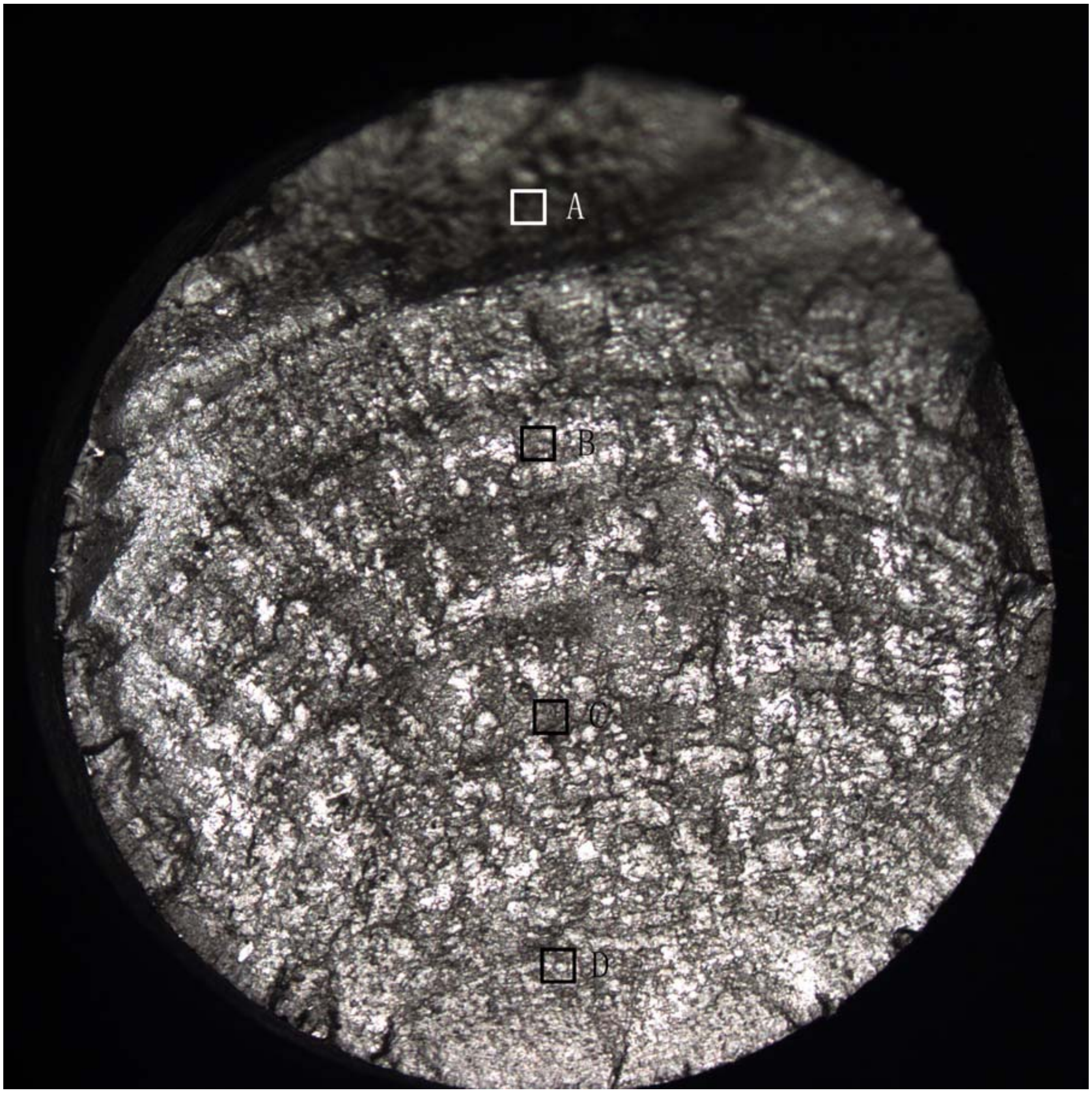

Figure 4-9: Fracture Section of MMFX II at Strain Amplitude 1.172% (R = -1)

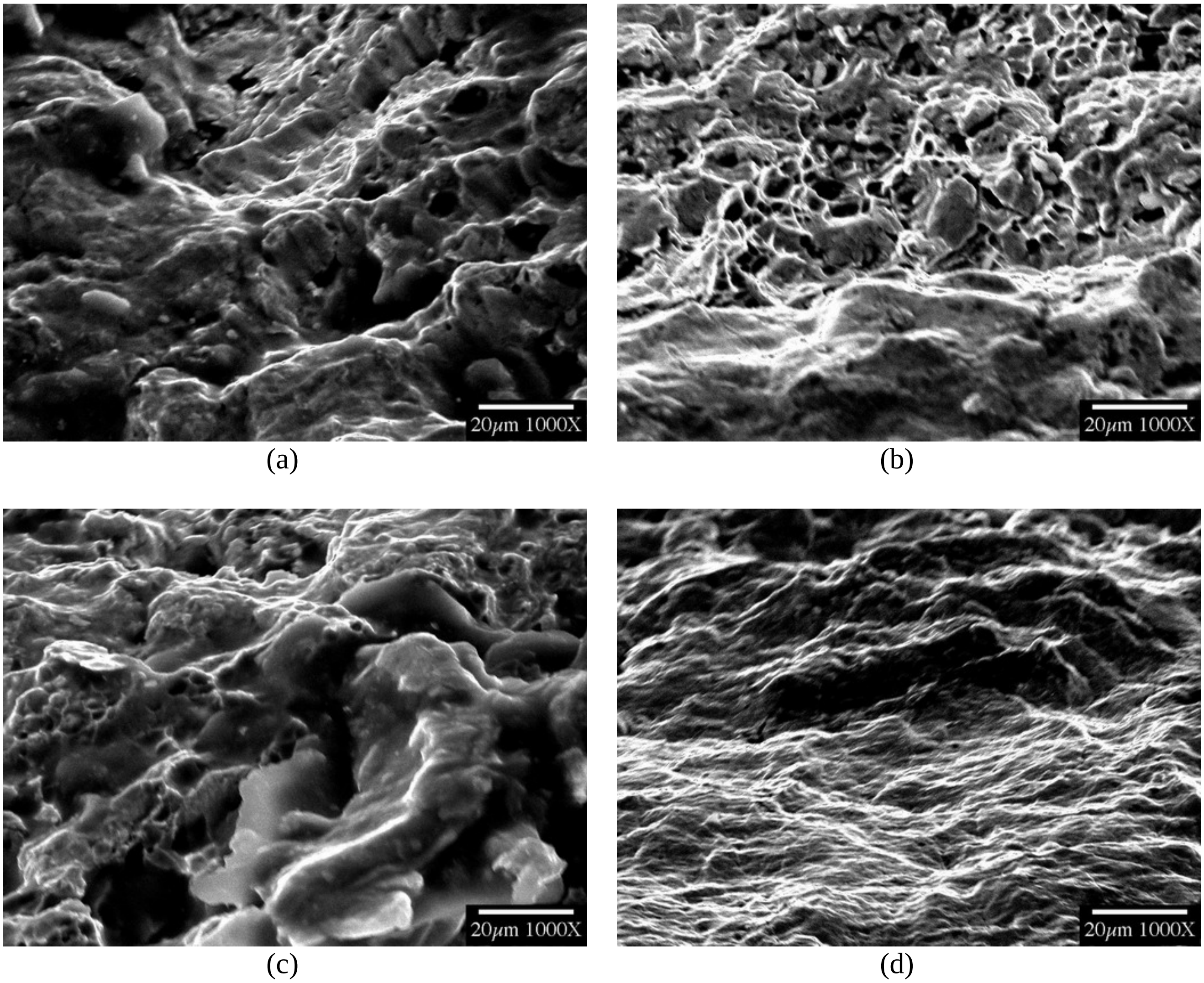

Figure 4-10: Electron Microscope Pictures for Fracture Section of MMFX II at Strain Amplitude 1.172% (R = -1)
(a). Zoomed in Area A in Figure 4-9
(b). Zoomed in Area B in Figure 4-9
(c). Zoomed in Area C in Figure 4-9
(d). Zoomed in Area D in Figure 4-9

4.2 Summary of the Fatigue Features of the Experimental Specimens

Five fracture sections from different types of steel investigated are shown in Figures 4-1, 4-3, 4-5, 4-7, and 4-9, respectively. Figures 4-2, 4-4, 4-6, 4-8 and 4-10 are the corresponding electron microscope pictures of zoomed in areas that have been marked in Figures 4-1, 4-3, 4-5, 4-7, and 4-9, respectively. The brown stain in the upper middle area in the fracture section in Figure 4-5 is the grease left by the specimen ends cut. And the light yellow stain in the lower middle part of the fracture section in Figure 4-7 is part of the rubber band that had melted at the end of the test. The beach mark of the three types of stainless steel is more obvious compared to A706 G60 and MMFX II. The Fracture surface of A706 G60 (Figure 4-7) is smoother than the rest of the steels investigated. Among the three types of stainless steel, fracture surfaces of Enduramet 32 (Figure 4-1) and 316LN (Figure 4-3) are typical and the fatigue characteristics are distinct, while those of 2205 duplex (Figure 4-5) are different. Taking the lower parts of the surfaces for example, the beach mark for Enduramet 32 and 316LN is finer compared to 2205 duplex; and that of 2205 duplex is flatter than Enduramet 32 as well as 316LN stainless. Metal fatigue first happened at the bottom of the sections with smooth surfaces and small radial beach marks. As the cyclic reverse loading continues, micro cracks occur, propagate and nucleate to form major cracks, and then the major cracks propagate across the section from bottom to the top. Coarse areas at the top demonstrate that those were the places where the specimens finally fractured. A certain amount of fracture sections of the low-cycle fatigue test specimens are almost perpendicular to the longitudinal direction of the specimens, while the others are slanted, which shows that the shear lips do affect the growth of the crack, and further study about the influence of the shear lips on the crack growth should be carried out in the future research work. With the increase of the strain amplitude, the beach marks on the fatigue specimens’ fracture section tend to be more and more visible with naked eye observation.

CHAPTER 5
REFERENCES

ACI Committee. (2005). *Building Code Requirements for Structural Concrete (ACI 318-05) and Commentary (ACI 318-05)*, American Concrete Institute, Farmington Hills, MI.

ASTM. (2004). *ASTM Annual Book*, American Society for Testing and Materials, West Conshohocken, PA.

Coffin, L.F.. (1954). “A Study of the Effects of Cyclic Thermal Stresses on a Ductile Metal”, Trans. ASME, Vol. 76.

Heiyantuduwa, R., A., W.G., and Mackechnie, J. R.. (2006). “Performance of a Penetrating Corrosion Inhibitor in Concrete Affected by Carbonation-Induced Corrosion”, *Journal of Materials in Civil Engineering* @ ASCE/November/December 2006.

Mander, J.B., Panthake, F.D. and Kasalanati, A.. (1994). “Low-Cycle Behavior of Reinforcing Steel”, *Journal of Material in Civil Engineering*, Vol. 6, No. 4, pp. 453-468..

Manson, S.S.. (1953). “Behavior of Materials under Conditions of Thermal Stress”, *Heat Transfer Symposium*, University of Michigan Engineering Research Institute.

Pellissier-Tanon, A., Bernard, J.L., Amzallag, C. and Rabbe, P..(1982). “Evaluation of the Resistance of Type 316 Stainless Steel against Progressive Deformation”, *Low-Cycle Fatigue and Life Prediction, ASTM STP 770*, pp. 69-80.

Sakumoto, Y., T.N., Matsuzaki, A.. (1996). “High-Temperature Properties of Stainless Steel for Buiding Structures”, *J. Struct. Engrg*, 122(4).

Smith, F.N.. (2007). “The Use of Stainless Steel Reinforcement”, *Concrete Engineering International*, Vol. 11, No. 2, pp. 25-27.

Stephens, Ralph I., Fatemi, Ali., Stephens, Robert R. and Fuchs, Henry O.. (2001). *Metal Fatigue in Engineering*, Second Edition, John Wiley & Sons, Inc., New York, NY.